

Discovery of 5-Chloro-*N*²-[(1*S*)-1-(5-fluoropyrimidin-2-yl)ethyl]-*N*⁴-(5-methyl-1*H*-pyrazol-3-yl)-pyrimidine-2,4-diamine (AZD1480) as a Novel Inhibitor of the Jak/Stat Pathway

Stephanos Ioannidis,^{*,†,‡} Michelle L. Lamb,^{†,‡} Tao Wang,^{†,‡} Lynsie Almeida,[†] Michael H. Block,[†] Audrey M. Davies,[†] Bo Peng,[†] Mei Su,[†] Hai-Jun Zhang,[†] Ethan Hoffmann,[§] Caroline Rivard,[§] Isabelle Green,^{||} Tina Howard,^{||} Hannah Pollard,^{||} Jon Read,^{||} Marat Alimzhanov,[‡] Geraldine Bebernitz,[‡] Kirsten Bell,[‡] Minwei Ye,[‡] Dennis Huszar,[‡] and Michael Zinda[‡]

[†]Department of Cancer Chemistry, [‡]Department of Cancer Bioscience and [§]Department of Drug Metabolism and Pharmacokinetics, AstraZeneca R&D, Boston, Massachusetts, United States, and ^{||}Discovery Enabling Capabilities and Sciences—Cells, Protein & Structural Sciences, AstraZeneca, Alderley Park, Cheshire, SK10 4TG, United Kingdom. [†]These authors have contributed equally to the preparation of this manuscript.

Received September 1, 2010

The myeloproliferative neoplasms, polycythemia vera, essential thrombocythemia, and idiopathic myelofibrosis are a heterogeneous but related group of hematological malignancies characterized by clonal expansion of one or more myeloid lineages. The discovery of the Jak2 V617F gain of function mutation highlighted Jak2 as a potential therapeutic target in the MPNs. Herein, we disclose the discovery of a series of pyrazol-3-yl pyrimidin-4-amines and the identification of **9e** (AZD1480) as a potent Jak2 inhibitor. **9e** inhibits signaling and proliferation of Jak2 V617F cell lines *in vitro*, demonstrates *in vivo* efficacy in a TEL-Jak2 model, has excellent physical properties and preclinical pharmacokinetics, and is currently being evaluated in Phase I clinical trials.

Introduction

The Jak (Janus-associated kinase) family consists of four nonreceptor tyrosine kinases, Tyk2^a, Jak1, Jak2, and Jak3, which play a critical role in cytokine and growth factor mediated signal transduction.¹ The cytosolic receptor-associated Jaks are activated by cytokine or growth factor engagement, resulting in downstream activation of associated signaling pathways, chief among which are the Stat family of transcription factors, comprising Stat1, Stat2, Stat3, Stat4, Stat5a, Stat5b, and Stat6. Pharmacological inhibition of Jak2 became an intense focus for small molecule drug discovery efforts after the discovery of a single activating somatic mutation in the pseudokinase (Janus Homology 2, JH2) domain of Jak2 in the myeloproliferative neoplasms (MPNs).^{2–5} The MPNs, primarily comprising essential thrombocythemia (ET), polycythemia vera (PV), and myelofibrosis (MF), are a heterogeneous but related group of hematological malignancies characterized by clonal expansion of one or more myeloid lineages. Among these, MF represents the greatest unmet medical need and has been the starting point for clinical trials of Jak2 inhibitors. Typical clinical features of MF include marked symptomatic splenomegaly, progressive anemia, and

constitutional symptoms including weight loss, fever, and night sweats. Morbidity and mortality commonly occur as a result of infection, thrombohemorrhagic events, portal hypertension, organ failure, and leukemic transformation. INCB-018424 (**1**),⁶ TG101348 (**2**),⁷ CYT387 (**3**),⁸ and CEP-701 (**4**)⁹ are among the Jak inhibitors that are being evaluated in man (Figure 1). Collectively, they have shown dramatic reversal of splenomegaly and alleviation of constitutional symptoms, but evidence for significant impact on the natural course of the disease has been lacking.¹⁰

Herein, we describe the discovery of a series of pyrazol-3-yl pyrimidin-4-amines as Jak2 inhibitors and structure–activity relationships of this series at R₁, R₃, and X (Figure 2). The detailed biological and pharmacokinetic evaluation of our lead compounds will also be described. This work culminated in the discovery and evaluation of **9e** as a potent and selective ATP-competitive Jak2 inhibitor that is currently in phase I clinical trials.

Chemistry

The synthetic route for the preparation of 2,4-diamino substituted pyrimidines is illustrated in Scheme 1. Aminopyrazoles **6a–d** were attached regioselectively to the 4-position of the pyrimidine ring upon treatment of an alcoholic solution of 2,4-dichloropyrimidines **5a–c** with base at ambient temperature. The desired 2-chloro-*N*-(1*H*-pyrazol-3-yl)pyrimidin-4-amine intermediates **7** were isolated in almost quantitative yield after simple extraction of the reaction mixture. The preparation of the intermediate 2-chloro-5-methyl-*N*-(5-methyl-1*H*-pyrazol-3-yl)pyrimidin-4-amine (X = Me, **7f**) required heating of the ethanolic solution at reflux, presumably due to the reduced electrophilicity of 2,4-dichloro-5-methylpyrimidine **5d**.

*To whom correspondence should be addressed. Tel.: (781) 839-4556. Fax: (781) 839-4630. E-mail: stephanos.ioannidis@astrazeneca.com.

^aAbbreviations: CDK2, cyclin-dependent kinase 2; DIAD, diisopropylazodicarboxylate; DIPEA, diisopropylethyl amine; DMA, dimethylacetamide; dppf, 1,1'-bis(diphenylphosphino)ferrocene; D5W, 5% dextrose (w/v) in water; ET, essential thrombocythemia; HPMC, hydroxypropylmethylcellulose; Jak2, Janus kinase 2; Jak1, Janus kinase 1; Jak3, Janus kinase 3; MF, idiopathic myelofibrosis; mpk, mg/kg; MPNs, myeloproliferative neoplasms; PEG, polyethylene glycol; PV, polycythemia vera; Stat, signal transducers and activators of transcription; pStat, phosphorylated signal transducers and activators of transcription; tStat, total signal transducers and activators of transcription; Tyk2, tyrosine kinase 2.

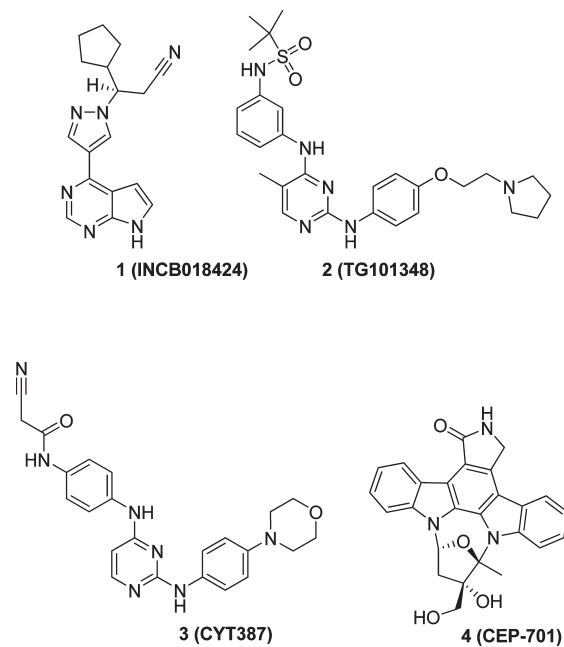


Figure 1. Jak inhibitors in the clinic.

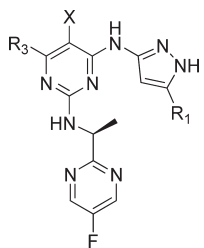


Figure 2. Pyrazol-3-yl pyrimidin-4-amines as Jak2 inhibitors.

Finally, reaction of (*S*)-5-fluoropyrimidin-2-yl-ethanamine hydrochloride¹¹ (*S*)-8 with 4-substituted-2-chloropyrimidines **7a–f** and **7i–l** under forcing conditions in the presence of DIPEA afforded the desired 2,4-disubstituted pyrimidines **9a–f** and **9i–l**.

The synthesis of the heteroaromatic alcohol **12** is illustrated in Scheme 2. Palladium-catalyzed cyanation of the commercially available 2-chloro-5-fluoropyrimidine proceeded smoothly to afford the corresponding 5-fluoropyrimidine-2-carbonitrile **10**. The synthetic route was completed by Grignard addition of methylmagnesium bromide to the nitrile followed by reduction of the intermediate ketone **11** to yield the desired alcohol **12** in almost quantitative yield.

Heating a solution of **12** with 2,5-dichloro-*N*-(5-methyl-1*H*-pyrazol-3-yl)pyrimidin-4-amine (**7e**) in presence of NaO^t-Bu overnight yielded the desired oxygen-substituted pyrimidines **9g** and **9h** as a mixture of enantiomers, which was readily separable by chiral purification (Scheme 3; see Figure S1 for chiral purification information).

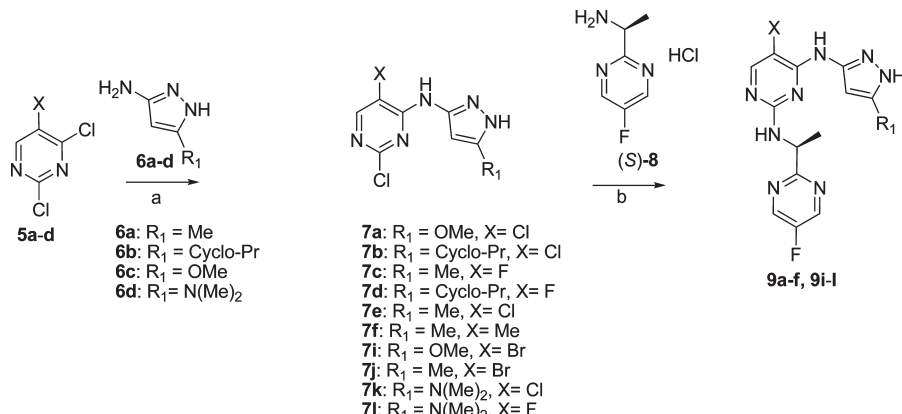
In the case of 2,4,6-trisubstituted pyrimidines, the desired analogues were generated by first exposing the 2,4,6-trichloropyrimidines to an ethanolic solution of the pyrazol-4-yl amines **6a** and **6c** in the presence of base (e.g., DIPEA) followed by nucleophilic aromatic substitution at the C-2 position of the pyrimidine core with (*S*)-8. The regioselectivity of the latter aromatic substitution was influenced by the C-5 substituent of the pyrimidine B-ring (for definition, see Table 1). The absence of substituent (X = H) at C-5 usually led to the

exclusive formation of the desired regio-isomer, while the presence of a chloro (X = Cl) substituent typically gave a mixture (3:1 to 2:1 ratio) in favor of the desired (*S*)-5,6-dichloro-*N*²-(1-(5-fluoropyrimidin-2-yl)ethyl)-*N*⁴-(1*H*-pyrazol-3-yl)-pyrimidine-2,4-diamine intermediates **15**. Exposure of the C-5 hydrogen- and chloro-substituted 6-chloro-*N*⁴-(1*H*-pyrazol-3-yl)pyrimidine-2,4-diamine intermediates (**15a,c,d,f**) to morpholine furnished the target molecules **16a,c,d,f** (Scheme 4). However, when the C-5 substituent was fluorine, reaction with (*S*)-8 favored the C-6 regio-isomer. Although the two corresponding regio-isomers could be readily separated by flash column chromatography, the overall yield of the desired regio-isomer was poor. An alternative route (Scheme 5) was therefore pursued where reaction of **14b** and **14e** with morpholine proceeded smoothly to afford the intermediates **17a** and **17b**, respectively. Microwave irradiation of **17a,b** in the presence of the chiral (*S*)-8 amine hydrochloride gave **16b** and **16e** in good yield (Scheme 5). While the reaction with morpholine again resulted in a mixture of C-4 and C-6 substituted intermediates, the use of morpholine conserved the precious chiral amine. Trichloropyrimidines **13a** and **13c** are commercially available, while **13b** was prepared according to previously reported procedures.¹²

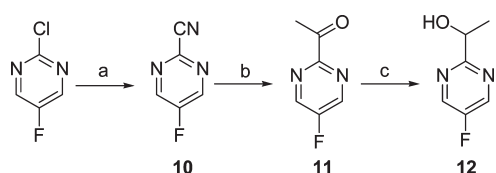
As depicted in Scheme 6, the methoxy aminopyrazole **6c** could be readily synthesized from the commercially available 3-amino-5-hydroxypyrazole via Mitsunobu reaction.¹¹ The synthesis of dimethylamino-substituted aminopyrazole **6d** was carried out starting from methyl dimethylthiocarbamate **18**. The thiocarbamate was accessible after treatment of carbon disulfide with dimethylamine under aqueous basic conditions (aq. NaOH). Reaction of the lithium anion of acetonitrile (prepared by exposure of the latter to *n*-BuLi) with **18** followed by quenching of the intermediate thiol with MeI furnished 3-(dimethylamino)-3-(methylthio)acrylonitrile **19** as a mixture of geometric isomers (*E* and *Z*). Subsequent formation of the pyrazole ring **6d** was accomplished in moderate yield on treatment of the diastereomeric mixture of **19** with hydrazine.

Results and Discussion

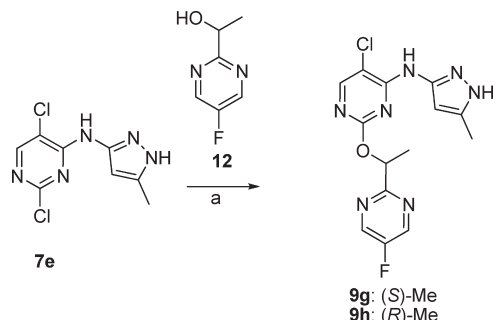
SAR Development. It was our hope that modifying the size of the R₁ substituent would have an influence on modulating inhibitory activity against Jak2 because of the proximity to the relatively large, aliphatic side chain of the methionine gatekeeper residue. In order to test this hypothesis, several R₁ substituents were examined (Table 1). Comparing the Jak2 enzymatic inhibition of the closely related analogues **9a**, **9b**, **9e**, and **9k** at Km ATP was inconclusive and failed to discriminate among the methoxy **9a**, cyclopropyl **9b**, and methyl **9e** analogues.¹³ The cyclopropyl and methyl analogues gave IC₅₀ values below the detection limit of the assay, with the methoxy-substituted analogue estimated to be slightly less active. The dimethylamine substituent in **9k** was less well tolerated; however, the compound was still a single-digit nanomolar inhibitor. Likewise, the enzymatic data of close analogues **9c**, **9d**, and **9l** (X = F) as well as of **9i** with **9j** (X = Br) prevented us from establishing the preferred substituent at R₁. Thus, to better differentiate the activity of these analogues against Jak2, testing at a higher concentration of ATP (5 mM) was utilized.¹⁴ We presumed that using this concentration, which is at the high end of ATP concentration in the cell, as opposed to Km, would allow us to more accurately discriminate among potent closely related analogues. It was also expected that the Jak2 high ATP data

Scheme 1. Preparation of 2,4-Diamino Substituted Pyrimidines^a

^a Reagents and conditions: (a) For **5a**, X = Cl; **5b**, X = F; **5c**, X = Br, Et₃N, EtOH, 0 °C → 25 °C; for **5d**, X = Me, Et₃N, EtOH, 60 °C. (b) For **9a**, DIPEA, n-BuOH, 110 °C; **9b–f**, DIPEA, n-BuOH, 120 °C microwave; **9i–l**: DIPEA, n-BuOH, 165 °C, microwave.

Scheme 2. Preparation of Racemic 1-(5-Fluoropyrimidin-2-yl)-ethanol **12**^a

^a Reagents and conditions: (a) Pd₂(dba)₃, Zn(CN)₂/Zn, dppf; (b) MeMgBr, THF, 0 °C; (c) NaBH₄, MeOH, 0 °C.

Scheme 3. Preparation of 2-Alkoxy Pyrimidin-4-amines^a

^a Reagents and conditions: (a) NaO'Bu, t-BuOH, 90 °C; then chiral purification.

would more effectively predict the potential cellular activity. Hence, the observed data in our primary cellular assay employing TEL-Jak2 in Ba/F3 cells¹³ should correlate well with the corresponding enzyme data at high ATP. From Table 1, it can be seen that indeed, in this particular series, potent activity at high ATP did translate into cellular potency. In addition, by considering both the Jak2 high ATP and TEL-Jak2 data we were able to determine that the methyl group was preferred for interaction with the Jak2 gatekeeper residue.

Our strategy in the development of Jak2 inhibitors has been to build in selectivity against Jak3, in order to avoid the immunosuppression associated with Jak3 deficiency. Hence, a Jak3 high ATP (5 mM) enzyme assay was introduced in order to better evaluate selectivity in the series, by comparison to Jak2 high ATP assay.¹⁴ As indicated in Table 1, a significant level of selectivity against Jak3 was observed in the series. This has been attributed to the 5-fluoro substituent on the pyrimidine C-ring and its unfavorable interaction

with the Jak3 binding site (vide infra). Interestingly, the methoxy (**9a** and **9i**) and dimethylamine (**9k** and **9l**) substituted compounds may show improved selectivity against Jak3, although possibly at the expense of Jak2 activity. The methyl group seems to achieve the optimum balance between Jak2 activity and selectivity versus Jak3, at both the biochemical and cellular levels.

Further exploration of structure–activity relationships involved variations of the C-5 substituent X of the central pyrimidine ring (B-ring), as depicted in Table 1. From the biochemical data, Me, Br, F, and Cl substituents at this position are all tolerated. In this instance, the high ATP Jak2 data were not able to distinguish among molecules due to their high potency, and prioritization could only be accomplished after using data from the TEL-Jak2 cellular assay. Compounds **9c**, **9e**, **9f**, and **9j** demonstrated a combination of favorable enzymatic and cellular activities together with selectivity over Jak3, however without preference for any substituent with respect to this selectivity. The former progressed through our cascade, while the bromo analogue (X = Br) **9j** was not profiled further due its increased lipophilicity (data not shown) over the fluoro (**9c**, X = F), chloro (**9e**, X = Cl), and methyl (**9f**, X = Me) analogues.

It is noteworthy that, although switching the nitrogen linker (Y) between B-ring and C-ring from NH to O resulted in a potent Jak2 inhibitor **9g** at the biochemical level, this enzymatic activity did not secure the desired level of activity in the TEL-Jak2 cellular assay.¹⁵ In addition, based upon examples such as **9g** and **9h**, it became apparent that the stereochemistry at the benzylic center was crucial for activity.

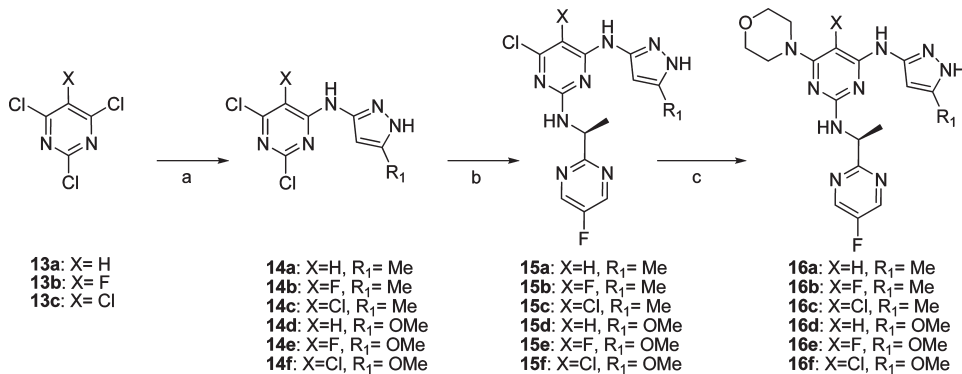
Introduction of Substituents at the C-6 Position of Pyrimidine B-Ring Oriented toward the Solvent Channel. Cognizant of the potential for improvement of Jak2 activity and modulation of the overall properties by substitution at the C-6 position of the pyrimidine B-ring, due to the potential access to the solvent channel,¹⁶ we elected to explore analogues **16a–c**. Incorporation of a C-6 morpholine moiety resulted in further improvements in cellular potency as shown in Table 2.

We then sought to reevaluate the effects of having an OMe group at the R₁ position for analogues with morpholine occupying the solvent channel. We wanted to explore the combination of the C-6 morpholine with the 5-methoxy pyrazol-3-amine, potentially providing compounds with improved cellular potency compared to the des-morpholino

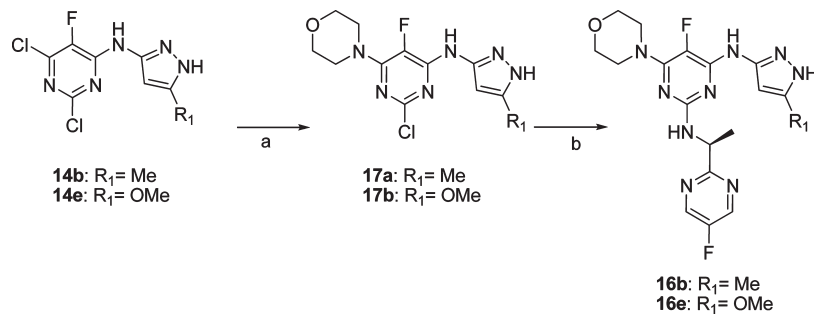
Table 1. Biochemical and Cellular Data of Pyrazol-3-yl pyrimidin-4-amine Analogues **9a–l**

cmpds	R ₁	R ₂	X	Y	Jak2 IC ₅₀ (μ M) ^{a,b}	Jak2 (High ATP) IC ₅₀	Jak3 (High ATP) IC ₅₀	TEL-Jak2 GI ₅₀
						(μ M) ^{b,c}	(μ M) ^{b,c}	(μ M) ^{b,d}
9a	OMe	(S)-Me	Cl	NH	0.003	0.108	> 30	0.41
9b	Cyclo-Pr	(S)-Me	Cl	NH	< 0.003	ND ^e	ND	0.15
9c	Me	(S)-Me	F	NH	< 0.003	0.005	5.25	0.23
9d	Cyclo-Pr	(S)-Me	F	NH	0.003	ND	ND	0.25
9e	Me	(S)-Me	Cl	NH	< 0.003	0.058 ^f	1.36 ^f	0.06
9f	Me	(S)-Me	Me	NH	< 0.003	0.004	8.35	0.096
9g	Me	(S)-Me	Cl	O	< 0.003	0.021	12.73	0.17
9h	Me	(R)-Me	Cl	O	0.346	1.3	> 30	> 10
9i	OMe	(S)-Me	Br	NH	0.004	0.108	> 30	0.59
9j	Me	(S)-Me	Br	NH	< 0.003	0.010	4.59	0.089
9k	NMe ₂	(S)-Me	Cl	NH	0.009	0.488	> 30	1.2
9l	NMe ₂	(S)-Me	F	NH	0.016	0.815	> 30	2.2

^a Measured at K_m ATP; for experimental details, see ref 13. ^b All values are an average of at least two independent dose-response curves. ^c For experimental details, see ref 14. ^d For experimental details, see ref 13. ^e Denotes not tested. ^f These data were generated according to the procedure reported in ref 19. When tested in the assay reported in ref 13, Jak2 IC₅₀ = 0.008 μ M, Jak3 IC₅₀ = 3.63 μ M.

Scheme 4. Preparation of 2,4,6-Trisubstituted Pyrimidines^a

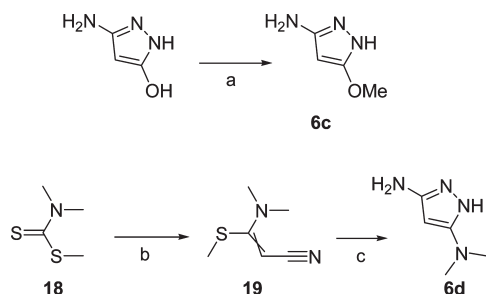
^a Reagents and conditions: (a) **6a** or **6c**, Et₃N, EtOH, 0 °C → 25 °C; (b) (S)-8 hydrochloride, DIPEA, EtOH, 70 °C; (c) DIPEA, n-BuOH, 120 °C, microwave.

Scheme 5. Synthetically Preferred Route for 5-Fluoro-2,4,6-Trisubstituted Pyrimidines^a

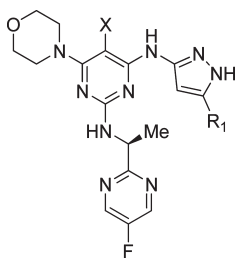
^a Reagents and conditions: (a) Morpholine, DIPEA, n-BuOH, 80 °C; (b) (S)-8 hydrochloride, DIPEA, n-BuOH, 190 °C, microwave.

analogues **9a** and **9i**. This hypothesis was less than fruitful, and the cellular activity of **16d–f** was much lower than the activity of the corresponding methyl analogues. It seems that, in this particular case, the methoxy substituent may be

bulky enough to lead to a steric clash with the thiomethyl side-chain of the methionine gatekeeper of Jak2 kinase resulting in less than optimum potency in comparison to the C-5 methyl matched pairs. Again, the Jak3 potency

Scheme 6. Preparation of Pyrazoles **6c** and **6d**^a

^a Reagents and conditions: (a) MeOH, DIAD, PPh₃, DCM, 0 °C; (b) CH₃CN, n-BuLi, -78 °C → 25 °C, then MeI, 0 °C; (c) H₂NNH₂, EtOH, 85 °C.

Table 2. Biochemical and Cellular Data of (*S*)-*N*²-(1-(5-Fluoropyrimidin-2-yl)ethyl)-6-morpholino-*N*⁴-(1*H*-pyrazol-3-yl)pyrimidine-2,4-diamine Analogues **16a–f**

compd	R ₁	X	Jak2 IC ₅₀	Jak2 (High ATP)	Jak3 (High ATP)	TEL-Jak2
			(μM) ^a	IC ₅₀ (μM) ^a	IC ₅₀ (μM) ^a	GI ₅₀ (μM) ^a
16a	Me	H	<0.003	<0.003	0.03	0.005
16b	Me	F	<0.003	<0.003	>30	0.013
16c	Me	Cl	<0.003	0.009	11.8	0.017
16d	OMe	H	0.010	0.030	0.20	0.073
16e	OMe	F	0.004	0.008	30.5	0.24
16f	OMe	Cl	0.004	0.090	2.96	1.30

^a All values are an average of at least two independent dose-response curves.

seemed to be controlled by the B-ring C-5 substituent, as indicated in Table 2, and not greatly influenced by the nature of the R₁ substituent. The absence of C-5 substituent (X = H) tends to shift the Jak3 activity into the nanomolar range, indicating that achievement of decent selectivity between Jak2 and Jak3 requires such substitution.

Pharmacokinetic Properties of Lead Compounds. Having identified leads showing excellent in vitro Jak2 inhibitory activity, we carried out an evaluation of the pharmacokinetic (PK) properties of these compounds in rats. Prior to in vivo profiling, the metabolic stability of the leads in rat liver microsomes was determined (see Table 3). From these data, it was predicted that the compounds would exhibit reasonable metabolic stability in vivo, and indeed, analogues **9c**, **9e**, **9f**, and **16a,b** showed low clearance when dosed intravenously (i.v.) in rats. Surprisingly, the chloro analogue **16c** was found to be highly cleared and exhibited a higher volume of distribution than the close analogues **16a** and **16b**. The basis of this difference is unclear, but the involvement of an alternative metabolic clearance pathway is a possibility. Compound **9e** also exhibited the longest half-life when administered i.v. in rat, while **9f** and **16b** displayed reasonably good half-lives (~2 h) and the other three analogues displayed a shorter half-life (≤ 1 h). All compounds demonstrated good solubility at physiological pH ($> 460 \mu\text{M}$) and low lipophilicity as assessed by logD_{7.4} measurements (< 2.60).

Table 3. Rat Microsomal Stability^a and PK Properties^b of Lead Compounds

compd	CL _{int} μL/min/mg	F%	CL _{obs} mL/min/kg	V _{dss} (L/kg)	T _{1/2} (h)
9c	10	100	12	0.8	0.85
9e	11	47	8.9	3.6	4.7
9f	25	100	18	2.4	1.9
16a	10	64	18	1.4	1.1
16b	NT	34	14	1.7	1.9
16c	16	20	221	4.6	0.36

^a For experimental details, see Experimental Section. ^b Han Wistar rat male; 10 mg/kg p.o. (0.1% HPMC); 3 mg/kg i.v. (40% DMA/40% PEG/20% saline).

Table 4. Mouse^a and Dog^b Pharmacokinetic Profile of **9e**

species	route	CL _{obs} (mL/min/kg)	T _{1/2} (hours)	V _{dss} (L/kg)	AUC (μM·h)	F%
mouse	i.v.	13.5	1.5	1.1		
	p.o.		2.0		57.6 ^c	100
dog	i.v.	2.0	6.9	1.0		
	p.o.		8.5		350 ^d	100

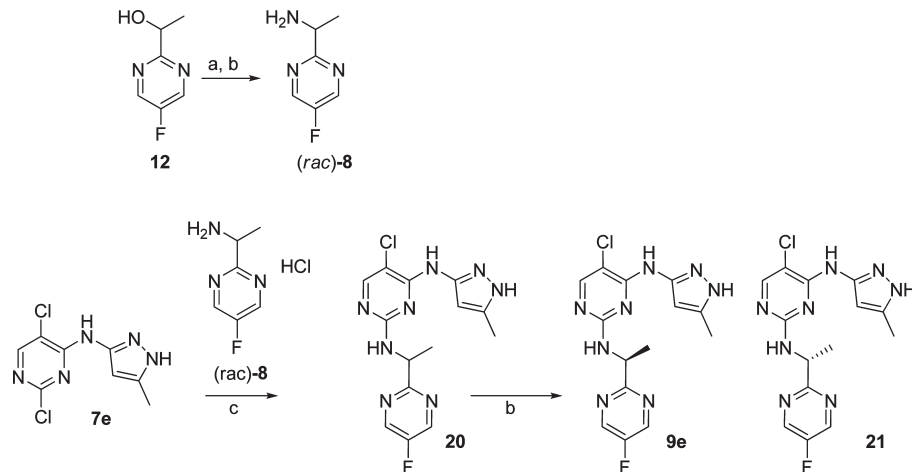
^a CD-1 mice female; 10 mg/kg p.o. (0.1% HPMC); 3 mg/kg i.v. (40% DMA/40% PEG/20% saline). ^b Beagle dog male; 10 mg/kg p.o. (0.1% HPMC, pH 2); 2.5 mg/kg i.v. (20% TEG/D5W). ^c AUC_{0→12 h}. ^d AUC_{0→24 h}.

Due to its excellent PK profile in rats together with the good cellular activity and enzymatic selectivity versus Jak3, we decided to progress **9e** into further in vivo studies and were gratified to observe an excellent PK profile in both mouse and dog (Table 4). The long half-life observed in dog and the excellent oral bioavailability in both species suggested possible full absorption and minimal first-pass metabolism following oral administration in both preclinical species.

Biological and Pharmacokinetic Evaluation of (*R*)-Enantiomer 21. To ensure that the (*S*)-stereochemistry in **9e** resulted in improved biological activity, the synthesis of (*R*)-enantiomer **21** was initiated (Scheme 7). Commencing from the previously reported alcohol **12**,¹⁷ formation of the desired racemic benzylic-like azide proceeded via conversion of the alcohol into the corresponding methanesulfonate and subsequent displacement with sodium azide. The azide was converted to the target amine (*rac*)-**8** via hydrogenation under standard conditions. The racemic material **20** was readily prepared upon heating 2,5-dichloro-*N*-(5-methyl-1*H*-pyrazol-3-yl)pyrimidin-4-amine (**7e**) with (*rac*)-**8** in a microwave. The two antipodes, **9e** and **21**, were readily separable by chiral purification (Supporting Information Figure S3).

Screening **21** in our biochemical and cellular assays indicated that stereochemistry has an effect on activity, as discussed above for **9g** and **9h**. Examining the PK properties of **21** in rat showed that there are differences between the enantiomers in the overall profile, particularly increased clearance and shorter half-life (Table 5).

Crystal Structure of 9e with the Kinase Domain of JAK2. The interaction of **9e** within the adenine binding site was confirmed by an X-ray structure with a Jak2 construct containing the JH1 (ATP-binding) domain. It was necessary to carry out isolation, purification, and crystallization of this construct in the presence of staurosporine. Subsequent displacement of staurosporine with the more potent **9e** afforded suitable crystals for X-ray analysis. As indicated in Figure 3, the pyrazole interacts with the hinge via a donor–acceptor–donor hydrogen-bonding motif with the protein backbone

Scheme 7. Preparation (*rac*)-**8** and **21**^a

^a Reagents and conditions: (a) i. MsCl, Et₃N, DCM, 0 °C; ii. NaN₃, DMF; (b) H₂, Pd/C, 25 °C; (c) DIPEA, *n*-BuOH, 120 °C, microwave.

Table 5. Biological and Pharmacokinetic Evaluation^a of **21**

Jak2 μ M (K_m ATP) ^b	TEL-Jak2 μ M ^b	CL (mL/min/kg)	$T_{1/2}$ (hours)	V_{dss} (L/kg)	AUC _{0–24 h} (μ M·h) p.o.
0.031	11	19	2.9	3.0	33.5

^a Han Wistar rat male; 10 mg/kg p.o. (0.1% HPMC); 3 mg/kg i.v. (40% DMA/40% PEG/20% saline). ^b Average of at least two independent dose-response curves.

atoms of leucine (L932) and glutamate (E930). The methyl group of the pyrazole is 3.6 Å from the terminal carbon of methionine 929, which explains the observed preference for methyl rather than larger substituents at this position.

Placement of the methyl at the chiral center of **9e** near the aliphatic side chain of valine 863 and glycine 856 in the P-loop (glycine-rich loop, not shown) contributes to the preference for (*S*)-Me over the *R*-enantiomer. The fluoro-pyrimidine ring occupies the hydrophobic pocket above L983 as shown in Figure 3, and the fluoro substituent is well-accommodated due to the presence of a glycine residue (G993) in Jak2 just prior to the activation loop “DFG-motif”. Interestingly, the difference of the amino acid backbone between Jak2 and Jak3¹⁸ (alanine, A966) at this position may be a factor in the selectivity against Jak3 observed in this series (Figure 4). It is likely that a steric clash between the fluoro substituent and the methyl side chain of alanine in Jak3 would result in tilting of the ring away from its optimal interaction within the ATP-binding site, hence the observed selectivity.

Kinase Selectivity. Evaluation of **9e** against a Millipore kinase panel, of 82 different kinases, has been previously reported and demonstrated Jak2 kinase activity inhibition with an IC₅₀ of < 0.003 μ M (Table 6).¹⁹

In cells, induction of mitotic block was assessed as a phenotypic end point of Aurora A inhibition.²⁰ Changes in the G2/M phase population of the cell cycle were only observed following treatment of SW620 colorectal adenocarcinoma cells with 3.3 μ M of **9e** for 24 h (Supporting Information Figure S2). Thus, **9e** demonstrated significant cellular selectivity for Jak2 versus the antiproliferative activity of Aurora A/B inhibition.

Likewise, the concentration-dependent autophosphorylation of TrkA in the MCF10A-Δ cell line²¹ was evaluated upon treatment with **9e** and showed > 12-fold selectivity for Jak2 against TrkA in the cellular context.

Cellular Profiling. As previously described,¹⁹ **9e** potently inhibits the growth of the Ba/F3 TEL-Jak2 cell line in an MTS tetrazolium colorimetric assay, with a GI₅₀ of 0.06 μ M. This antiproliferative activity has been shown to be tightly correlated with the inhibition of Stat5 phosphorylation (pStat5) in Ba/F3 TEL-Jak2 cells (IC₅₀ of 0.046 μ M). We have also shown that **9e** exhibits significant selectivity against Jak3 and Tyk2, and to a smaller extent against Jak1, when tested in Ba/F3 cells transfected with the kinase domains of these JAK family members (Jak1, Jak3, and Tyk2) fused to the TEL domain, as demonstrated by growth inhibition data (Table 7).¹⁹ To establish the potential of **9e** to have an effect in a more clinically relevant setting, its effect on human hematopoietic cell lines identified to carry the Jak2 V617F mutation was examined.²² Thus, testing in the SET-2 cell-line (a human megakaryoblastic cell line derived from an ET patient heterozygous for V617F), UKE-1 (homozygous for V617F), and HEL (homozygous and amplified copies of V617F) revealed significant growth inhibition of these lines as shown by the GI₅₀ data given in Table 7.

Further studies in the SET-2 cell line showed that both Stat5 and Stat3 phosphorylation was inhibited (IC₅₀: 0.025 μ M and 0.023 μ M, respectively) upon treatment with **9e**, indicating that the SET-2 GI₅₀ correlates closely with pStat inhibition (Figure 5).

In a similar manner, the effect of **9e** on Stat5 phosphorylation in UKE-1 cells was examined and the IC₅₀ again found to be in close correlation with the observed GI₅₀ (Figure 6).

In contrast, in the HEL (human erythroleukemia) cell line **9e** inhibits Stat5 phosphorylation with an IC₅₀ of 0.041 μ M and Stat3 phosphorylation with an IC₅₀ of 0.08 μ M (Figure 7). The discordance between pStat IC₅₀ values (0.041–0.08 μ M) and the GI₅₀ value (0.39 μ M) may result at least in part from amplification of the Jak2 locus in this cell line, as well as secondary changes associated with leukemic transformation.

Furthermore, duration of exposure experiments in HEL cells demonstrated onset of inhibition of Stat3 and Stat5

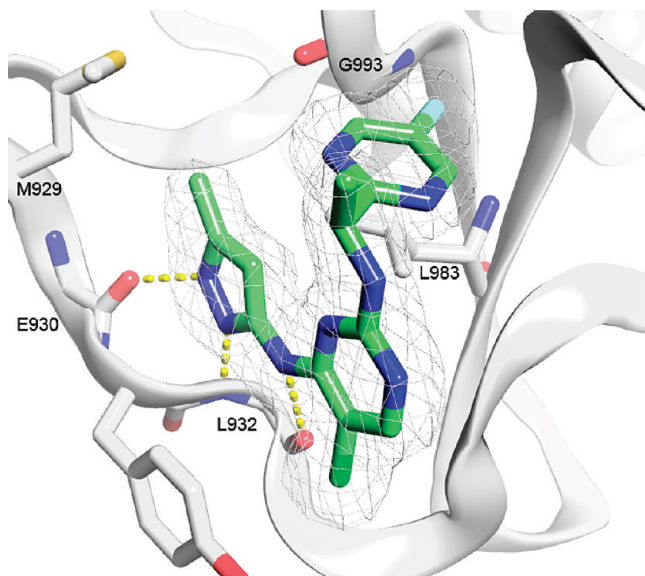


Figure 3. Crystal structure (pdb:2XA4) of compound **9e** bound to Jak2 kinase. Carbon atoms for **9e** are shown in green. The protein backbone cartoon is represented in white. Selected atoms for the hinge region (on the left) from gatekeeper M929 to L932 as well as G993 (at the top) are represented as sticks. Refined electron density ($2f_0f_C$) contoured at $1.0\ \sigma$ for the inhibitor is represented as wire mesh. The glycine-rich loop has been removed for clarity.

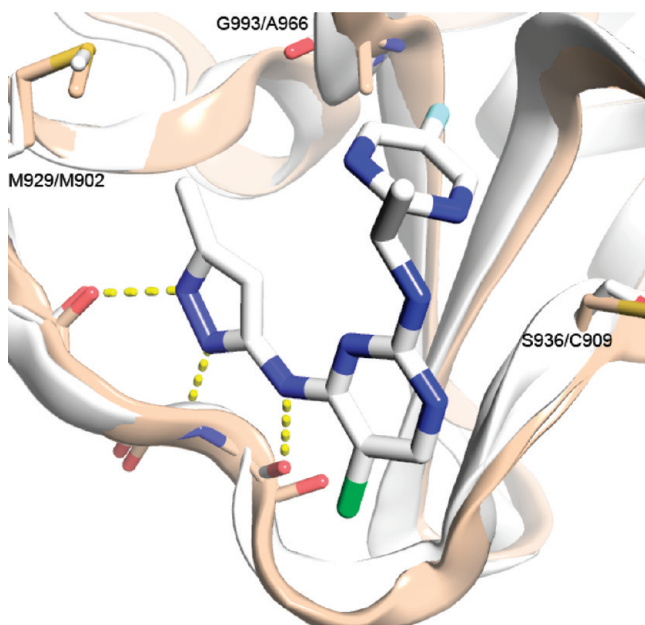


Figure 4. Contribution of G993/A966 residue to the observed selectivity of **9e** for Jak2 versus Jak3. Protein backbone atoms of 2XA4 (white) and 1YVJ (wheat) overlaid and represented as cartoon. Hydrogen bonds between compound **9e** and the protein are shown in yellow. Selected residues from the two structures have been represented as sticks and labeled with Jak2/Jak3 residue names and numbers.

phosphorylation within 5 min of treatment with $0.3\ \mu\text{M}$ of **9e** and maximal inhibition of phosphorylation within 30–60 min of drug treatment. Recovery of phosphorylation was also rapid and was complete within 10–15 min after drug removal for both Stats (Figure 8).

9e Demonstrates a Clear Pharmacodynamic (PD) Effect in Mouse Allograft Model. As a biomarker of Jak2 inhibition in

Table 6. Kinase Profiling of **9e**^a

target	enzyme fold selectivity
Jak2	1
TrkA	1
Aurora-A	3
Flt-4	5
FGFR1	9
ARK5	10
JAK3	16
FAK	19
Axl	19
ALK4	27
Ret	30
ALK	33
Flt3	42
LKB1	63

^a Jak2 inhibitory activity was measured to be $<0.003\ \mu\text{M}$, while for TrkA, inhibitory activity was measured to be $0.003\ \mu\text{M}$. The numbers given for enzyme fold selectivity correspond to the minimum possible selectivity.

Table 7. Inhibition of Janus Kinase Family Members Driven Cellular Proliferation in Engineered Ba/F3 Cell Lines and Cell Lines Carrying the Clinically Relevant V617F Mutation by **9e**

cmpd	GI ₅₀ μM	fold selectivity
Ba/F3 TEL-Jak2	0.06	-
Ba/F3 TEL-Jak3	2.1	35
Ba/F3 TEL-Jak1	0.7	12
Ba/F3 TEL-Tyk2	2.0	33
SET-2 (V617F)	0.016	
UKE-1 (V617F)	0.054	
HEL	0.39	

vivo, we measured pStat5 levels in splenic tissue from mice implanted with murine Ba/F3 TEL-Jak2 cells (Supporting Information Figure S4). Single doses of **9e** at 5–30 mg/kg were given by oral gavage and individual mice sacrificed at different time points post-dose. Almost complete inhibition of Stat5 phosphorylation was observed for at least 12 h following a single 30 mg/kg dose of **9e** as determined by quantification of pStat5 levels in spleen lysates by Western blot. At the 10 mg/kg dose, pStat5 was inhibited by >70% for at least 8 h but was largely recovered by 12 h. At the 5 mg/kg dose level, about 90% inhibition of pStat5 was observed at 2 h post-dose, but only approximately 50% inhibition was maintained at 6 h (Figure 9). Thus, dose-dependent duration of pStat5 inhibition was observed with **9e** in the *in vivo* model.

9e Shows Tumor Growth Inhibition in the Mouse Ba/F3 TEL-Jak2 Allograft Efficacy Model. Ba/F3 TEL-Jak2 cells were genetically modified to express the firefly luciferase gene (*luc*), so that tumor cell growth could be readily monitored and quantified *in vivo* by bioluminescent imaging (BLI) using a Xenogen IVIS imaging system.²³ Nude mice were implanted with the Ba/F3 TEL-Jak2-*luc* cells and randomized into treatment groups one day later based on BLI. **9e** was given orally at 30 or 50 mg/kg twice daily, starting on day 3 after tumor cell implantation. In the vehicle-treated mice, the intensity of bioluminescent signal increased exponentially during the first 7 days, in agreement with rapid proliferation of the tumor cells *in vivo* (data not shown). In contrast, we observed a significant dose-dependent inhibition of tumor cell growth in **9e**-treated animals as indicated by a relative reduction in light emission compared to the vehicle-treated mice (Figure 10A). On day 9, there was a 44-fold reduction in bioluminescent signal intensity in

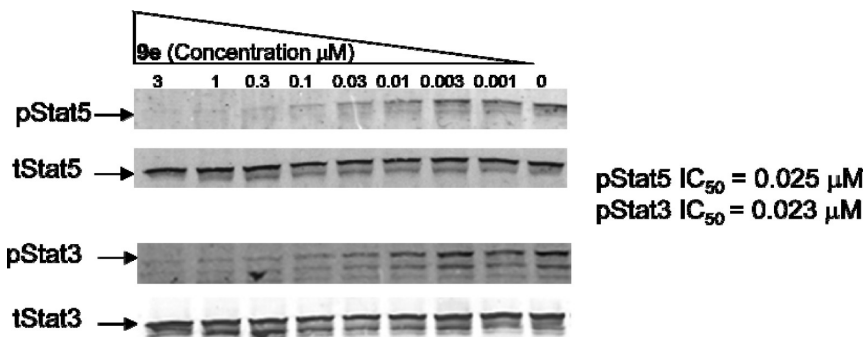


Figure 5. Dose-dependent inhibition of pStat5 (phosphorylated Stat5) and pStat3 (phosphorylated Stat3) **9e** and total proteins (tStat5 and tStat3) in SET-2 human megakaryoblastic cells. Cells were treated with decreasing concentration of **9e** for 1 h, harvested, and run on SDS-PAGE; phosphorylated and total Stat proteins were assayed by Western Blot and quantitated using Licor Odyssey imager.¹⁹

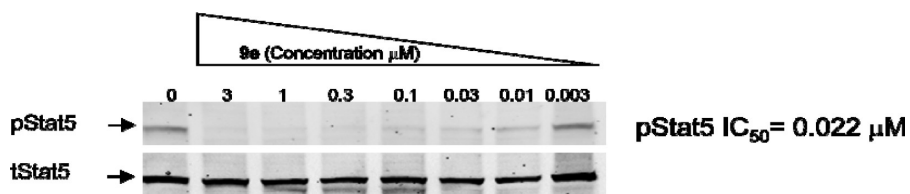


Figure 6. Dose-dependent inhibition of pStat5 (phosphorylated Stat5) by **9e** and total proteins (tStat5) in UKE-1 (homozygous for V617F) human hematopoietic cells. Cells were treated with decreasing concentration of **9e** for 1 h, harvested, and run on SDS-PAGE; phosphorylated and total Stat proteins were assayed by Western Blot and quantitated using Licor Odyssey imager.¹⁹

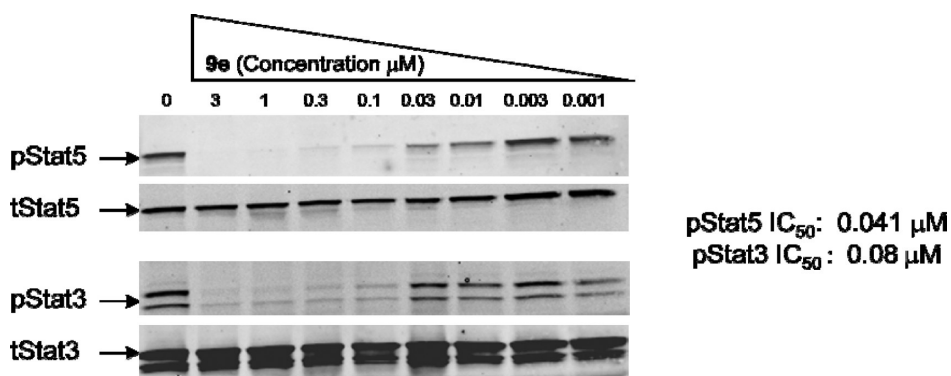


Figure 7. Dose-dependent inhibition of pStat5 (phosphorylated Stat5) and pStat3 by **9e** and total proteins (tStat5 and tStat3) in HEL (human erythroleukemia) cells. Cells were treated with decreasing concentration of **9e** for 1 h, harvested, and run on SDS-PAGE; phosphorylated and total Stat proteins were assayed by Western blot and quantitated using Licor Odyssey imager.¹⁹

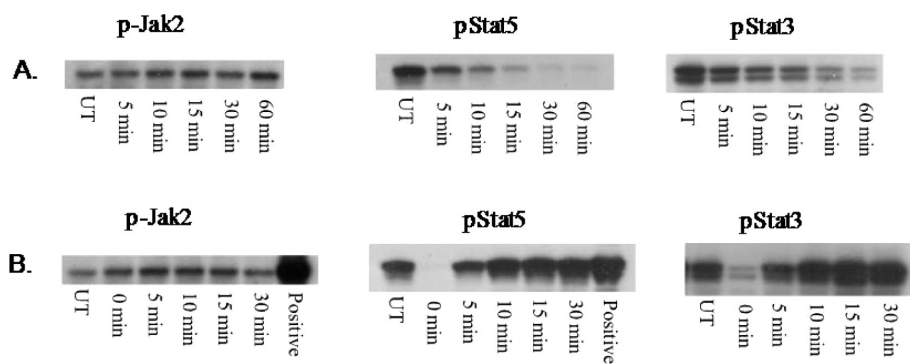


Figure 8. (A) Kinetic response of pStat3 and pStat5 to the addition of 0.3 μM of **9e**. Reduction of the pStat5 levels was apparent at 15 min, and complete inhibition was observed at 60 min upon addition of **9e**. pStat3 expression could be partially inhibited after 60 min incubation with **9e**, while p-Jak2 signaling did not change upon addition of **9e**. (B) Both pStat5 and pStat3 signaling recovered 5 min after washout of **9e**. p-Jak2 denotes phosphorylated Jak2 and UT denotes untreated.

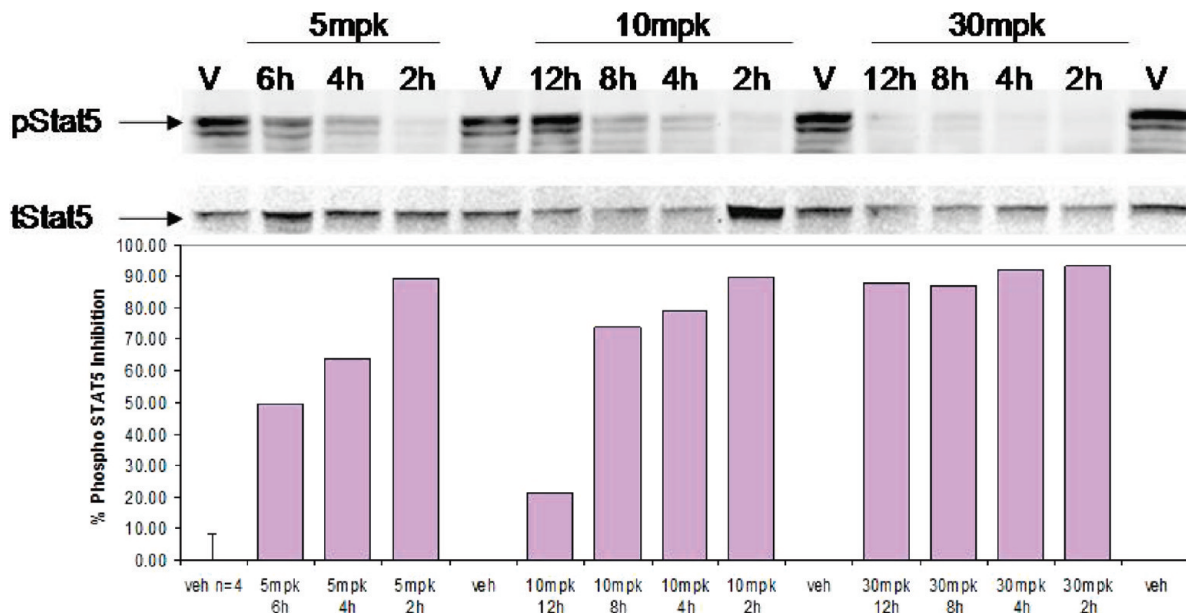


Figure 9. Dose-dependent modulation of pStat5 levels in splenic tissue after a single dose of **9e** in a Ba/F3 TEL-Jak2 mouse model. The bars represent the mean percentage (%) inhibition in phosphorylation of Stat5 (\pm SD, $n = 3$ for each dose and each time point) and are calculated using vehicle (V, veh) and control inhibitor for establishing maximum and minimum values. The Western blots and quantitation described with the Ba/F3 engineered cells were performed as previously described.¹³

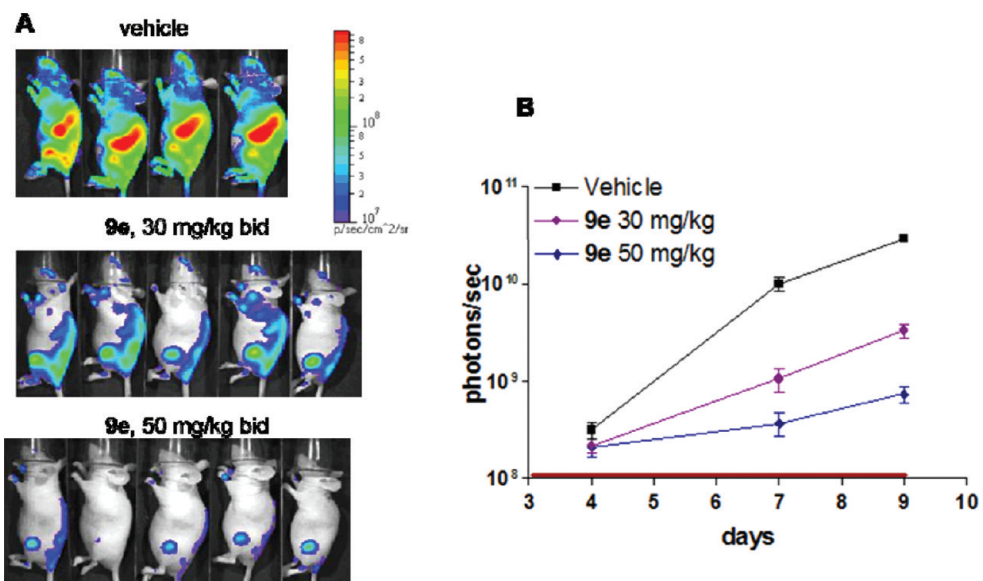


Figure 10. Effect of **9e** treatment on Ba/F3 TEL-Jak2–luc cell growth in vivo. (A) Groups of animals were treated with either vehicle ($n = 8$) or **9e** at 30 mg/kg twice daily ($n = 5$) or **9e** at 50 mg/kg twice daily ($n = 5$) starting on day 3 post-tumor cell implantation. Pseudocolor images representing luciferase-emitted light intensity superimposed over photographs of the tumor-bearing mice from each treatment group. The images were acquired on day 9 post-tumor cell implantation. The color scheme for the luminescence intensity is shown by the color bar. (B) Total bioluminescent signal intensity over each mouse body was determined on days 4, 7, and 9 and averaged per time point and treatment group. Means \pm SE were plotted using GraphPad Prism 4 software.

the 50 mg/kg dose group and approximately 9-fold reduction in the 30 mg/kg dose group compared to the control animals (Figure 10B).

Conclusions

We have described the discovery of a series of pyrazol-3-yl pyrimidin-4-amines as potent inhibitors of the Jak/Stat pathway. Screening in biochemical and cellular assays allowed us to select **9e** (AZD1480) for extensive preclinical evaluation. This compound showed good selectivity for Jak2 and Jak1

within the Jak family and across many other tested kinases. **9e** suppressed activation of the Jak2/Stat pathway in low nanomolar concentrations in hematopoietic lineages carrying the V617F mutation. The excellent pharmacokinetic properties of this compound prompted us to explore the pharmacodynamic effect in a TEL-Jak2 model in a dose-dependent manner. No significant weight loss or other adverse effects were observed upon dosing, and a single dose of 30 mg/kg was sufficient to prevent phosphorylation of Stat5 for over 12 h. An efficacy study with TEL-Jak2 luciferase cells demonstrated

dose-dependent tumor growth inhibition at well-tolerated doses. The attractive preclinical profile of **9e** resulted in progression to clinical evaluation in myelofibrosis.

Experimental Section

Chemistry. ¹H NMR spectra were recorded on either Bruker 300 or 400 MHz NMR spectrometers using deuterated DMSO (DMSO-*d*₆) unless otherwise stated. Temperatures are given in degrees Celsius (°C); operations are carried out at room temperature or ambient temperature, that is, in the range 18–25 °C. Chemical shifts are expressed in parts per million (ppm, δ units). Coupling constants are given in units of hertz (Hz). Splitting patterns describe apparent multiplicities and are designated as s (singlet), d (doublet), dd (doublet–doublet), t (triplet), q (quartet), m (multiplet), and br s (broad singlet). Mass spectroscopy analyses were performed with an Agilent 1100 equipped with Waters columns (Atlantis T3, 2.1 × 50 mm, 3 μm or Atlantis dC18, 2.1 × 50 mm, 5 μm) eluted with a gradient mixture of H₂O–acetonitrile with formic acid and ammonium acetate. The purity determination of all reported compounds was performed with an Agilent 1100 equipped with Waters columns (Atlantis T3, 2.1 × 50 mm, 3 μm; or Atlantis dC18, 2.1 × 50 mm, 5 μm) eluted for >10 min with a gradient mixture of H₂O–acetonitrile with formic or trifluoroacetic acid at wavelengths of 220, 254, and 280 nm. All compounds analyzed were ≥95% pure. Reverse-phase chromatography was performed with Gilson systems using a YMC-AQC18 reverse-phase HPLC column with dimension 20 mm/100 and 50 mm/250 in water/MeCN with 0.1% TFA as mobile phase. Elemental analyses (C, H, N) were performed by QTI, P.O. Box 470, 291 Route 22 East, Salem Industrial Park – Bldg 5, Whitehouse, NJ 08888. Most of the reactions described were monitored by thin-layer chromatography on 0.25 mm E. Merck silica gel plates (60F-254), visualized with UV light or LC/MS. Flash column chromatography was performed on ISCO MPLC Combi-flash systems (4700 Superior Street, Lincoln, NE, USA) unless otherwise mentioned using silica gel cartridges. SFC (super critical fluid chromatography) refers to Analytical SFC (ASC-1000 Analytical SFC System with Diode Array Detector) and/or Preparative SFC (APS-1000 AutoPrep Preparative SFC), obtained from SFC Mettler Toledo AutoChem, Inc. (7075 Samuel Morse Drive Columbia, MD 21046, USA) and used according to the manufacturer's instruction.

5-Methoxy-1*H*-pyrazol-3-amine (6c). To a solution of 3-amino-5-hydroxypyrazole (50.0 g) in CH₂Cl₂ (800 mL) was added triphenyl phosphine (155.6 g) and the resulting mixture cooled to 0 °C. Diisopropyl azodicarboxylate (117.6 mL) was added dropwise over a period of 35 min (maintaining an internal temperature <2 °C) to give a slurry. The reaction mixture was then stirred at 0 °C for 1 h. A beige precipitate formed after 20 min. MeOH (50 mL) was then added dropwise over a period of 15 min at 0 °C as the slurry thinned considerably to give a lighter yellow slurry. The reaction mixture was then stirred at 0 °C for 1 h and then warmed slowly to ambient temperature over a period of 2 h. The reaction mixture was then stirred at ambient temperatures for 22 h when it was filtered to remove precipitates. The filtrate was dried over MgSO₄ and concentrated under reduced pressure to give a yellow–orange oil. Purification by flash column chromatography (5–10% MeOH/CH₂Cl₂) afforded the title compound as a waxy solid (yield: 40%). ¹H NMR (300 MHz) δ: 4.67 (s, 1H) 3.61 (s, 3H). *m/z*: 114. The hydrochloride salt was obtained after dissolving 5-methoxy-1*H*-pyrazol-3-amine in MeOH and dropwise treatment of the resulting mixture with a solution of HCl (4 N in dioxane). The mixture was allowed to stir at room temperature for 1 h, and evaporation of the volatiles under reduced pressure afforded the hydrochloride salt as white solid (yield: quantitative).

N⁵,N⁵-Dimethyl-1*H*-pyrazole-3,5-diamine (6d). A mixture of (2*E* and *Z*)-3-(dimethylamino)-3-(methylthio)acrylonitrile

(9.5 g) and hydrazine hydrate (10 mL) in ethanol (70 mL) was heated at 85 °C overnight. The volatiles were removed under reduced pressure, and the residue left was purified by flash column chromatography with a gradient of 0–10% methanol in CH₂Cl₂ with 1% NH₄OH to afford the title compound (yield: 69%) as thick oil. ¹H NMR (400 MHz) δ 9.51 (br, 1H), 4.67 (s, 1H), 2.62 (s, 6H). *m/z*: 127.

2,5-Dichloro-N-(5-methoxy-1*H*-pyrazol-3-yl)pyrimidin-4-amine (7a). To a solution of 5-methoxy-1*H*-pyrazol-3-amine (**6c**, 0.9 g) in absolute EtOH (20 mL) was added triethylamine (3.3 mL) and 2,4,5-trichloropyrimidine (1.4 g) at ambient temperature. The resulting solution was aged at room temperature for 12 h, whereupon it was partitioned between EtOAc and H₂O. The organic layer was washed with brine and dried over MgSO₄. The solvents were removed under reduced pressure to give the title compound as an oil, which crystallized upon standing (yield: 97%). *m/z*: 261.

Following a similar procedure to that of **7a**, the following compounds were synthesized.

2,5-Dichloro-N-(5-cyclopropyl-1*H*-pyrazol-3-yl)pyrimidin-4-amine (7b). From 5-cyclopropyl-1*H*-pyrazol-3-amine **6b** and 2,4,5-trichloropyrimidine (yield: 95%). *m/z*: 271.

2-Chloro-5-fluoro-N-(5-methyl-1*H*-pyrazol-3-yl)pyrimidin-4-amine (7c). From 5-methyl-1*H*-pyrazol-3-ylamine **6a** and 2,4-dichloro-5-fluoropyrimidine (yield: 97%). *m/z*: 228.

2-Chloro-N-(5-cyclopropyl-1*H*-pyrazol-3-yl)-5-fluoropyrimidin-4-amine (7d). From 5-cyclopropyl-1*H*-pyrazol-3-amine **6b** and 2,4-dichloro-5-fluoropyrimidine (yield: 95%). *m/z*: 254.

2,5-Dichloro-N-(5-methyl-1*H*-pyrazol-3-yl)pyrimidin-4-amine (7e). From 5-methyl-1*H*-pyrazol-3-ylamine **6a** and 2,4,5-trichloropyrimidine (yield: 95%). *m/z*: 245.

5-Bromo-2-chloro-N-(5-methoxy-1*H*-pyrazol-3-yl)pyrimidin-4-amine (7f). From 5-methoxy-1*H*-pyrazol-3-amine **6c** and 5-bromo-2,4-dichloropyrimidine (yield: 95%). *m/z*: 305.

5-Bromo-2-chloro-N-(5-methyl-1*H*-pyrazol-3-yl)pyrimidin-4-amine (7j). From 5-methyl-1*H*-pyrazol-3-amine **6a** and 5-bromo-2,4-dichloropyrimidine (yield: 95%). ¹H NMR (CDCl₃) 2.24 (s, 3H), 6.24 (s, 1H), 8.41 (s, 1H), 9.29 (s, 1H), 12.32 (s, 1H).

N⁵-(2-Chloro-5-fluoropyrimidin-4-yl)-N⁵,N⁵-dimethyl-1*H*-pyrazole-3,5-diamine (7l). From N⁵,N⁵-dimethyl-1*H*-pyrazole-3,5-diamine **6d** and 2,4-dichloro-5-fluoropyrimidine. ¹H NMR (400 MHz, 80 °C) 11.60 (br s, 1H), 10.26 (br s, 1H), 8.23 (s, 1H), 5.73 (s, 1H), 2.76 (s, 6H). *m/z*: 257.

N⁵-(2,5-dichloropyrimidin-4-yl)-N⁵,N⁵-dimethyl-1*H*-pyrazole-3,5-diamine (7k). From N⁵,N⁵-dimethyl-1*H*-pyrazole-3,5-diamine **6d** and 2,4,5-trichloropyrimidine. ¹H (400 MHz, 80 °C) 11.67 (br, 1H), 9.51 (br s, 1H), 8.34 (s, 1H), 5.68 (s, 1H), 2.76 (s, 6H). *m/z*: 273.

2-Chloro-5-methyl-N-(5-methyl-1*H*-pyrazol-3-yl)pyrimidin-4-amine (7f). To a solution of 2,4-dichloro-5-methylpyrimidine (1.25 g) in EtOH (30 mL) was added 5-methyl-1*H*-pyrazol-3-ylamine (**6a**, 0.75 mg) and DIPEA (2.8 mL), at room temperature. The mixture was heated at 70 °C overnight. The mixture was allowed to cool to room temperature whereupon a precipitate was observed. The title compound was collected by filtration under vacuum as a white solid (yield: 41%). ¹H NMR 12.17 (s, 1H), 9.30 (s, 1H), 7.97 (s, 1H), 6.37 (s, 1H), 2.25 (s, 3H), 2.13 (s, 3H). *m/z*: 224.

1-(5-Fluoropyrimidin-2-yl)ethanamine (*rac*)-8. A round-bottom flask containing 1-(5-fluoropyrimidin-2-yl)ethanol (**12**, 0.79 g) was charged with triethylamine (0.93 mL) and anhydrous CH₂Cl₂ (10 mL) at ambient temperature. The solution was cooled to 0 °C, and methanesulfonyl chloride (0.7 g) was added dropwise. The resulting mixture was allowed to stir at room temperature for 2 h, at which point the volatile components were removed under reduced pressure. The residue was dissolved in DMF (15 mL) and treated with sodium azide (0.7 g). The resulting mixture was stirred at room temperature for 60 h and was then partitioned between EtOAc and brine. The organic layer was collected, dried (Na₂SO₄), and evaporated under reduced pressure to dryness. The crude

material was purified by flash column chromatography with 50% EtOAc and hexanes gradient to afford 2-(1-azidoethyl)-5-fluoropyrimidine as a colorless oil (yield: 65% yield over two steps). GC-MS, 167 (M), 138 (M-N₂), 125 (M-N₃); ¹H NMR (CDCl₃) δ 8.60 (s, 2H), 4.60 (m, 1H), 1.65 (d, 3H).

A round-bottom flask containing 2-(1-azidoethyl)-5-fluoropyrimidine (0.6 g) was charged with 10% Pd/C (0.19 g) and was evacuated and backfilled with H₂ via a filled balloon. MeOH (10 mL) was added, and the mixture was stirred at room temperature for 3 h. The mixture was filtered through a plug of diatomaceous earth, which was subsequently washed well with MeOH. The filtrates were concentrated under reduced pressure to give the title compound as a pale yellow oil (yield: 99%). ¹H NMR (CDCl₃) δ 8.60 (s, 2H), 4.65 (br s 2H), 4.10 (m, 1H), 1.20 (d, 3H).

5-Chloro-N²-[(1S)-1-(5-fluoropyrimidin-2-yl)ethyl]-N⁴-(5-methoxy-1H-pyrazol-3-yl)pyrimidine-2,4-diamine (9a). A mixture of 2,5-dichloro-N-(5-methoxy-1H-pyrazol-3-yl)pyrimidin-4-amine (7a, 0.06 g) and (S)-1-(5-fluoropyrimidin-2-yl)ethanamine hydrochloride (S)-8 (0.04 g) in n-BuOH (0.8 mL) and DIPEA (0.13 mL) was heated at 110 °C overnight. The solvent was evaporated under reduced pressure, and the remaining material was separated between EtOAc and water, and the combined organic extract washed with brine and dried over MgSO₄. Evaporation of the solvent under reduced pressure gave a brown oil (0.06 g). Purification by reverse-phase chromatography (10–50% MeCN/H₂O 0.1% TFA, 15 min) afforded the trifluoroacetate salt of the title compound as a white solid (yield: 40%). ¹H NMR: 9.64 (s, 1H), 8.78 (d, 2H), 8.18 (s, 1H), 7.86 (s, 1H), 5.52 (s, 1H), 4.99–5.15 (m, 1H), 3.65 (s, 3H), 1.43 (d, 3H). *m/z*: 366.

5-Chloro-N⁴-(5-cyclopropyl-1H-pyrazol-3-yl)-N²-[(1S)-1-(5-fluoropyrimidin-2-yl)ethyl]pyrimidine-2,4-diamine (9b). A mixture of (S)-1-(5-fluoropyrimidin-2-yl)ethanamine hydrochloride (S)-8 (0.09 g), 2,5-dichloro-N-(5-cyclopropyl-1H-pyrazol-3-yl)pyrimidin-4-amine (7b, 0.13 g), and DIPEA (0.26 mL) in n-BuOH (2.5 mL) was heated in a sealed microwave vessel in a microwave reactor at 180 °C for 6 h. The solvent was removed under reduced pressure, and the residue was purified by reverse-phase chromatography (10–50% MeCN/H₂O 0.1% TFA, 15 min) to give the trifluoroacetate salt of the title compound (yield: 25%). ¹H NMR: 10.64 (s, 1H), 8.91 (s, 3H), 8.30 (s, 1H), 5.97 (s, 1H), 5.17 (s, 1H), 1.83–1.97 (m, 1H), 1.56 (d, 3H), 0.93–1.09 (m, 2H), 0.63–0.77 (m, 2H). *m/z*: 413.

5-Fluoro-N²-[(1S)-1-(5-fluoropyrimidin-2-yl)ethyl]-N⁴-(5-methyl-1H-pyrazol-3-yl)pyrimidine-2,4-diamine (9c). A mixture of (S)-1-(5-fluoropyrimidin-2-yl)ethanamine hydrochloride (S)-8 (95 mg), 2-chloro-5-fluoro-N-(5-methyl-1H-pyrazol-3-yl)pyrimidin-4-amine (7c, 0.11 g) and DIPEA (0.13 mL) in n-BuOH (2.5 mL) was heated in a sealed microwave vessel in a microwave reactor at 180 °C for 6 h. The solvent was removed under reduced pressure, and the residue was purified by reverse-phase chromatography (10–50% MeCN/H₂O, 0.1% TFA 15 min) to give the trifluoroacetate salt of the title compound (yield: 18%). ¹H NMR: 11.26 (s, 1H), 9.18–8.67 (m, 3H), 8.22 (s, 1H), 6.04 (s, 1H), 4.86–5.40 (m, 1H), 2.25 (s, 3H), 1.57 (d, 3H). *m/z*: 333.

N⁴-(5-Cyclopropyl-1H-pyrazol-3-yl)-5-fluoro-N²-[(1S)-1-(5-fluoropyrimidin-2-yl)ethyl]pyrimidine-2,4-diamine (9d). A mixture of (S)-1-(5-fluoropyrimidin-2-yl)ethanamine hydrochloride (S)-8 (0.09 g), 2-chloro-N-(5-cyclopropyl-1H-pyrazol-3-yl)-5-fluoropyrimidin-4-amine (7d, 0.13 g), and DIPEA (0.22 mL) in n-BuOH (2.5 mL) was heated in a sealed microwave vessel in a microwave reactor at 180 °C for 6 h. The solvent was removed under reduced pressure, and the residue was purified by reverse-phase chromatography (10–50% MeCN/H₂O, 0.1% TFA 15 min) to give the trifluoroacetate salt of the title compound (yield: 20%). ¹H NMR: 11.28 (s, 1H), 8.92 (s, 3H), 8.24 (s, 1H), 6.04 (s, 1H), 4.92–5.54 (m, 1H), 1.82–1.98 (m, 1H), 1.56 (d, 3H), 0.94–1.06 (m, 2H), 0.64–0.80 (m, 2H). *m/z*: 395.

5-Chloro-N²-[(1S)-1-(5-fluoropyrimidin-2-yl)ethyl]-N⁴-(5-methyl-1H-pyrazol-3-yl)pyrimidine-2,4-diamine (9e). A mixture of (S)-

1-(5-fluoropyrimidin-2-yl)ethanamine hydrochloride (S)-8 (0.08 g), 2,5-dichloro-N-(5-methyl-1H-pyrazol-3-yl)pyrimidin-4-amine (7e, 0.12 g) and DIPEA (0.14 mL) in n-BuOH (2.5 mL) was heated in a sealed microwave vessel in a microwave reactor at 180 °C for 6 h. The solvent was removed under reduced pressure, and the residue was purified by reverse-phase chromatography (10–50% MeCN/H₂O, 0.1% TFA 15 min) to give the trifluoroacetate salt of the title compound (yield: 50%). ¹H NMR: 10.34 (s, 1H), 8.91 (s, 3H), 8.30 (s, 1H), 5.94 (s, 1H), 4.96–5.34 (m, 1H), 2.25 (s, 3H), 1.56 (d, 3H). *m/z*: 350. Anal. (C₁₄H₁₄ClFN₈·0.4H₂O): C, calcd 48.21, found 47.96; H, calcd 4.04, found 4.05; N, calcd 32.13, found 30.67.

N²-[(1S)-1-(5-fluoropyrimidin-2-yl)ethyl]-5-methyl-N⁴-(5-methyl-1H-pyrazol-3-yl)pyrimidine-2,4-diamine (9f). A mixture of (S)-1-(5-fluoropyrimidin-2-yl)ethanamine (S)-8 (0.11 g), 2-chloro-5-methyl-N-(5-methyl-1H-pyrazol-3-yl)pyrimidin-4-amine (7f, 0.50 g), and DIPEA (0.225 mL) in anhydrous n-BuOH (2.1 mL) was heated in a sealed microwave vessel in a microwave reactor at 180 °C for 4 h. The solvent was removed under reduced pressure, and the residue was purified by reverse-phase chromatography (5–95% MeCN/H₂O 0.1% TFA, 15 min) to give the trifluoroacetate salt of the title compound (yield: 50%). ¹H NMR: 10.08 (s, 1H), 8.93 (s, 2H), 8.70 (s, 1H), 7.74 (s, 1H), 5.98 (s, 1H), 4.79–5.44 (m, 1H), 2.23 (s, 3H), 2.10 (s, 3H), 1.57 (d, 3H); *m/z*: 330.

(S)-5-Chloro-2-[1-(5-fluoropyrimidin-2-yl)ethoxy]-N-(5-methyl-1H-pyrazol-3-yl)pyrimidin-4-amine (9g) and (R)-5-Chloro-2-[1-(5-fluoropyrimidin-2-yl)ethoxy]-N-(5-methyl-1H-pyrazol-3-yl)pyrimidin-4-amine (9h). Sodium t-butoxide (2.9 g) was added to a solution of 2,5-dichloro-N-(5-methyl-1H-pyrazol-3-yl)pyrimidin-4-amine (7e, 3.7 g) and 1-(5-fluoropyrimidin-2-yl)ethanol (12, 4.3 g) in *t*-BuOH (10 mL). The resulting mixture was heated at 90 °C overnight and then was partitioned between H₂O and CH₂Cl₂. The organic layer was washed with saturated NH₄Cl_(aq) solution, H₂O, and brine. Purification by flash column chromatography (40% EtOAc/hexanes) afforded the title compounds as a mixture of enantiomers. ¹H NMR: 8.58 (s, 2H), 8.00 (s, 1H), 6.00 (s, 1H), 5.91 (m, 1H), 2.23 (s, 3H), 1.63 (d, 3H). *m/z*: 350.

The mixture was separated using chiral SFC. Column and solvent conditions: Column: Chiralcel AD-H, 250 × 20 mm, 5 μ . Modifier: 30% isopropanol, 0.1% dimethylethylamine. Flow rate: 60 mL/min. Oven: 40 °C. Outlet: 100 bar. Post-purification purity check: Chiral SFC using ultraviolet diode array. Column: Chiralcel AD-H, 250 × 4.6 mm. Conditions: 30% isopropanol, 0.1% dimethylethylamine. Flow rate: 3 mL/min; 15 min. Oven: 35 °C. Outlet: 120 bar.

9g was eluted first (yield: 16%) from the column with a retention time of 3.34 min, as detected using an ultraviolet diode array detector. **9h** was eluted second (yield: 15%) from the column with a retention time of 5.99 min, as detected using an ultraviolet diode array detector. Enantiomeric excess for both **9g** and **9h** was estimated to be >98%, using area percentage at 254 nm.

For **9g**, elemental analysis (C₁₄H₁₃ClFN₇O): C, calcd 48.08, found 48.04; H, calcd 3.75, found 3.74; N, calcd 28.03, found 27.82.

5-bromo-N²-[(1S)-1-(5-fluoropyrimidin-2-yl)ethyl]-N⁴-(5-methoxy-1H-pyrazol-3-yl)pyrimidine-2,4-diamine (9i). A mixture of 5-bromo-2-chloro-N-(5-methoxy-1H-pyrazol-3-yl)pyrimidin-4-amine (7i, 0.18 g) was added to a mixture of (S)-1-(5-fluoropyrimidin-2-yl)ethanamine hydrochloride (S)-8 (0.15 g), and DIPEA (0.14 mL) in anhydrous n-BuOH (2.5 mL) was heated in a sealed microwave vessel in a microwave reactor at 165 °C for 5 h. The reaction mixture was concentrated under reduced pressure, and the resulting residue was purified by flash column chromatography, eluting with 0–5% gradient of MeOH in DCM with 1% NH₄OH_(aq), to afford the title compound (yield: 40%). ¹H NMR: 12.03 (s, 1H), 9.38 (s, 1H), 8.82 (s, 2H), 8.12–7.97 (m, 2H), 5.60 (s, 1H), 5.13 (s, 1H), 3.75 (m, 3H), 1.49 (m, 3H). *m/z*: 409.

Compounds **9j–l** were prepared following a similar procedure to that described for (**9i**).

5-bromo-N²-[(1*S*)-1-(5-fluoropyrimidin-2-yl)ethyl]-N⁴-(5-methyl-1*H*-pyrazol-3-yl)pyrimidine-2,4-diamine (9j**).** From (*S*)-1-(5-fluoropyrimidin-2-yl)ethanamine hydrochloride (*S*)-**8** and 5-bromo-2-chloro-*N*-(5-methyl-1*H*-pyrazol-3-yl)pyrimidin-4-amine **7j** to afford the desired product (yield: 45%). ¹H NMR: 12.02 (s, 1H), 8.82 (s, 2H), 7.94 (s, 1H), 7.48 (s, 0.55H), 5.90 (s, 0.41H), 5.09 (s, 1H), 2.19 (m, 3H), 1.49 (m, 3H). *m/z*: 393.

5-chloro-N²-[5-(dimethylamino)-1*H*-pyrazol-3-yl]-N²-[(1*S*)-1-(5-fluoropyrimidin-2-yl)ethyl]pyrimidine-2,4-diamine (9k**).** From *N*³-(2,5-dichloropyrimidin-4-yl)-*N*⁵,*N*⁵-dimethyl-1*H*-pyrazole-3,5-diamine **7k** and (*S*)-1-(5-fluoropyrimidin-2-yl)ethanamine hydrochloride (*S*)-**8** to afford the title compound as a white solid (yield: 20%). ¹H NMR (CD₃OD): 8.77 (s, 2H), 8.26 (br, 1H), 5.35 (br, 1H), 3.49 (q, 1H), 3.11 (s, 6H), 1.72 (d, 3H); *m/z*: 378.

N⁴-[5-(dimethylamino)-1*H*-pyrazol-3-yl]-5-fluoro-N²-[(1*S*)-1-(5-fluoropyrimidin-2-yl)ethyl]pyrimidine-2,4-diamine (9l**).** From *N*³-(2-chloro-5-fluoropyrimidin-4-yl)-*N*⁵,*N*⁵-dimethyl-1*H*-pyrazole-3,5-diamine **9l** and (*S*)-1-(5-fluoropyrimidin-2-yl)ethanamine hydrochloride (*S*)-**8** to afford the title compound as a white solid (yield: 20%). ¹H NMR (CD₃OD): 8.77 (s, 2H), 8.23 (s, 1H), 5.32 (br, 1H), 3.92 (q, 1H), 3.13 (s, 6H), 1.71 (d, 3H); *m/z*: 362.

5-Fluoropyrimidine-2-carbonitrile (10**).** A 10 mL microwave vial was charged with 2-chloro-5-fluoropyrimidine (2.0 g), Pd₂(dba)₃ (0.55 g), dppf (0.7 g), zinc cyanide (1.1 g), and zinc dust (0.24 g). The flask was evacuated and backfilled with N₂ and anhydrous DMA (20 mL). The vial was mounted onto a Personal Chemistry microwave reactor and heated at 100 °C for 10 h. The reaction mixture was diluted with EtOAc and then washed with brine three times. The organic layer was obtained and evaporated to dryness under reduced pressure. The dried residue was purified by flash column chromatography, eluting with gradient 0–50% EtOAc and hexanes, to afford the title compound as a creamy solid (yield: 80%). GC-MS: 123 [M]⁺. ¹H NMR (CDCl₃) 8.80 (s, 2H).

1-(5-Fluoropyrimidin-2-yl)ethanone (11**).** To a solution of 5-fluoropyrimidine-2-carbonitrile (**10**, 2.5 g) in Et₂O (50 mL) at 0 °C was added dropwise a solution of MeMgBr (12 mL, 3.0 M in Et₂O). The resulting solution was stirred at this temperature for 30 min and was then allowed to warm to ambient temperature overnight. The mixture was quenched with a solution of saturated NH₄Cl_(aq) and extracted with Et₂O. The organic extracts were dried over MgSO₄, and evaporation under reduced pressure gave a colored residue. Purification by flash column chromatography, eluting with 3% MeOH/CH₂Cl₂, afforded the title compound (yield: 60%). ¹H NMR (CDCl₃): 8.75 (s, 2H), 2.77 (s, 3H).

1-(5-Fluoropyrimidin-2-yl)ethanol (12**).** NaBH₄ (12 mL, 3.0 M in Et₂O) was added slowly to a solution of 1-(5-fluoropyrimidin-2-yl)ethanone (**11**, 0.8 mg) in MeOH (40 mL) at 0 °C. The resulting solution was allowed to stir at room temperature for 30 min. The solvent was evaporated under reduced pressure, and the residue obtained was partitioned between H₂O and CH₂Cl₂. The organic layer was washed with saturated NH₄Cl_(aq) solution, H₂O, and brine. The organic extracts were dried over MgSO₄, and evaporation of the volatiles under reduced pressure gave the title compound (yield: 77%). ¹H NMR (CDCl₃): 8.59 (s, 2H), 4.96 (m, 1H), 3.79 (br s, 1H), 1.54 (d, 3H).

Compounds **14a–f** were prepared following a similar procedure to that described for **7a**.

2,6-Dichloro-*N*-(5-methyl-1*H*-pyrazol-3-yl)pyrimidin-4-amine (14a**).** From 2,4,6-trichloropyrimidine and 5-methyl-1*H*-pyrazol-3-amine **6a**. *m/z*: 245.

2,6-Dichloro-5-fluoro-*N*-(5-methyl-1*H*-pyrazol-3-yl)pyrimidin-4-amine (14b**).** From 2,4,6-trichloro-5-fluoropyrimidine and 5-methyl-1*H*-pyrazol-3-amine **6a**. *m/z*: 262.

2,5,6-Trichloro-*N*-(5-methyl-1*H*-pyrazol-3-yl)pyrimidin-4-amine (14c**).** From 2,4,5,6-tetrachloropyrimidine and 5-methyl-1*H*-pyrazol-3-amine **6a**. *m/z*: 277.

2,6-Dichloro-*N*-(5-methoxy-1*H*-pyrazol-3-yl)pyrimidin-4-amine (14d**).** From 2,4,6-trichloropyrimidine and 5-methoxy-1*H*-pyra-

zol-3-amine **6c**. ¹H NMR: 12.19 (s, 1H), 10.68 (s, 1H), 6.76 (s, 1H), 5.40 (s, 1H), 3.82 (s, 3H). *m/z*: 260.

2,6-Dichloro-5-fluoro-*N*-(5-methoxy-1*H*-pyrazol-3-yl)pyrimidin-4-amine (14e**).** From 2,4,6-trichloro-5-fluoropyrimidine and 5-methoxy-1*H*-pyrazol-3-amine **6c** (yield: 75%). *m/z*: 278.

2,5,6-Trichloro-*N*-(5-methoxy-1*H*-pyrazol-3-yl)pyrimidin-4-amine (14f**).** From 2,4,5,6-tetrachloropyrimidine and 5-methoxy-1*H*-pyrazol-3-amine **6c** (yield: 85%). *m/z*: 294.

The following compounds were synthesized following a similar procedure to that described for **9a**.

6-Chloro-N²-[(1*S*)-1-(5-fluoropyrimidin-2-yl)ethyl]-N⁴-(5-methyl-1*H*-pyrazol-3-yl)pyrimidine-2,4-diamine (15a**).** From 2,6-dichloro-*N*-(5-methyl-1*H*-pyrazol-3-yl)pyrimidin-4-amine **14a** and (*S*)-1-(5-fluoropyrimidin-2-yl)ethanamine hydrochloride (*S*)-**8**. *m/z*: 348.

(S)-6-chloro-5-fluoro-N²-(1-(5-fluoropyrimidin-2-yl)ethyl)-N⁴-(5-methyl-1*H*-pyrazol-3-yl)pyrimidine-2,4-diamine (15b**).** From 2,6-dichloro-5-fluoro-*N*-(5-methyl-1*H*-pyrazol-3-yl)pyrimidin-4-amine **14b** and (*S*)-1-(5-fluoropyrimidin-2-yl)ethanamine hydrochloride (*S*)-**8**. *m/z*: 367.

di(S)-5,6-dichloro-N²-(1-(5-fluoropyrimidin-2-yl)ethyl)-N⁴-(5-methyl-1*H*-pyrazol-3-yl)pyrimidine-2,4-diamine (15c**).** From 2,5,6-trichloro-*N*-(5-methyl-1*H*-pyrazol-3-yl)pyrimidin-4-amine **14c** and (*S*)-1-(5-fluoropyrimidin-2-yl)ethanamine hydrochloride. *m/z*: 383.

6-chloro-N²-(1-(5-fluoropyrimidin-2-yl)ethyl)-N⁴-(5-methoxy-1*H*-pyrazol-3-yl)pyrimidine-2,4-diamine (15d**).** From 2,6-dichloro-5-methoxy-*N*-(5-methyl-1*H*-pyrazol-3-yl)pyrimidin-4-amine **14d** and (*S*)-1-(5-fluoropyrimidin-2-yl)ethanamine hydrochloride (*S*)-**8**. ¹H NMR: 8.92 (s, 2H), 5.95 (s, 1H), 5.18 (s, 1H), 3.77 (s, 3H), 1.49 (d, 3H). *m/z*: 366.

(S)-6-chloro-5-fluoro-N²-(1-(5-fluoropyrimidin-2-yl)ethyl)-N⁴-(5-methoxy-1*H*-pyrazol-3-yl)pyrimidine-2,4-diamine (15e**).** From 2,6-dichloro-5-methoxy-*N*-(5-methoxy-1*H*-pyrazol-3-yl)pyrimidin-4-amine **14e** and (*S*)-1-(5-fluoropyrimidin-2-yl)ethanamine hydrochloride (*S*)-**8**. *m/z*: 383.

5,6-dichloro-N²-(1-(5-fluoropyrimidin-2-yl)ethyl)-N⁴-(5-methoxy-1*H*-pyrazol-3-yl)pyrimidine-2,4-diamine (15f**).** 2,5,6-Trichloro-*N*-(5-methoxy-1*H*-pyrazol-3-yl)pyrimidin-4-amine **14f** and (*S*)-1-(5-fluoropyrimidin-2-yl)ethanamine hydrochloride (*S*)-**8**. ¹H NMR: 9.87 (s, 1H), 8.88 (s, 2H), 8.78 (s, 1H), 8.38 (d, 1H), 5.62 (s, 1H), 5.06–5.17 (m, 1H), 3.77 (s, 3H), 1.49 (d, 3H). *m/z*: 399.

2-Chloro-5-fluoro-*N*-(5-methyl-1*H*-pyrazol-3-yl)-6-morpholin-4-ylpyrimidin-4-amine (17a**).** A mixture of morpholine (0.18 mL), 2,6-dichloro-5-fluoro-*N*-(5-methyl-1*H*-pyrazol-3-yl)pyrimidin-4-amine **14b** (0.5 g) and DIPEA (0.5 mL) in absolute ethanol (10 mL) was heated at 80 °C for 5 h. The solvent was removed under reduced pressure, and the residue was purified by reverse-phase chromatography (10–50% MeCN/H₂O with 0.1% TFA, 15 min) to give the trifluoroacetate salt of the title compound (yield: 29%). ¹H NMR: 12.05 (br s, 1H), 9.57 (s, 1H), 6.21 (s, 1H), 3.67 (t, 4H), 3.57 (t, 4H), 2.22 (s, 3H). *m/z*: 313.

2-Chloro-5-fluoro-*N*-(5-methoxy-1*H*-pyrazol-3-yl)-6-morpholin-4-ylpyrimidin-4-amine (17b**).** Prepared by a similar procedure as described above for **17a** using 2,6-dichloro-5-methoxy-*N*-(5-methyl-1*H*-pyrazol-3-yl)pyrimidin-4-amine **14e** as starting material (yield: 25%). ¹H NMR: 9.80 (s, 1H), 5.66 (s, 1H), 3.77 (s, 3H), 3.64–3.71 (m, 4H), 3.53–3.64 (m, 4H). *m/z*: 329.

N²-(1-(5-Fluoropyrimidin-2-yl)ethyl)-N⁴-(5-methyl-1*H*-pyrazol-3-yl)-6-morpholin-4-ylpyrimidine-2,4-diamine (16a**).** A mixture of 6-chloro-N²-(1-(5-Fluoropyrimidin-2-yl)ethyl)-N⁴-(5-methyl-1*H*-pyrazol-3-yl)pyrimidine-2,4-diamine (**15a**, 0.17 g), morpholine (0.09 mL) and DIPEA (0.13 mL) in *n*-BuOH (2.5 mL) was heated at 110 °C for 48 h. The solvent was removed under reduced pressure and the residue purified by reverse-phase chromatography (5–35% MeCN/H₂O with 0.1% TFA, 15 min) to give the trifluoroacetate salt of the title compound (yield: 40%). ¹H NMR: 11.19 (s, 1H), 9.28 (s, 1H), 8.74–9.03 (m, 3H), 5.81–5.83 (m, 1H), 5.73 (s, 1H), 4.98–5.24 (m, 2H), 3.58–4.12 (m, 6H), 2.39 (s, 3H), 1.54 (d, 3H). *m/z*: 436.

5-fluoro-N²-[(1*S*)-1-(5-fluoropyrimidin-2-yl)ethyl]-N⁴-(5-methyl-1*H*-pyrazol-3-yl)-6-morpholin-4-ylpyrimidine-2,4-diamine (16b). A mixture of (*S*)-1-(5-fluoropyrimidin-2-yl)ethanamine hydrochloride (**8**) (0.14 g), 2-chloro-5-fluoro-*N*-(5-methyl-1*H*-pyrazol-3-yl)-6-morpholin-4-ylpyrimidin-4-amine (**17a**, 0.3 g), and DIPEA (0.3 mL) in *n*-BuOH (5 mL) was heated in a sealed vessel in a microwave reactor at 180 °C for 9 h. The solvent was removed under reduced pressure and the residue purified by reverse-phase chromatography (2–40% MeCN/H₂O with 0.1% TFA, 15 min) to give the trifluoroacetate salt of the title compound (yield: 11%). ¹H NMR: 8.84 (s, 2H), 4.90–5.02 (m, 1H), 3.38–3.72 (m, 8H), 2.16 (s, 3H), 1.44 (d, 3H). *m/z*: 418.

(S)-5-chloro-N²-[(1-(5-fluoropyrimidin-2-yl)ethyl)-N⁴-(5-methyl-1*H*-pyrazol-3-yl)-6-morpholinopyrimidine-2,4-diamine (16c). A mixture of (*S*)-5,6-dichloro-*N*²-(1-(5-fluoropyrimidin-2-yl)ethyl)-*N*⁴-(5-methyl-1*H*-pyrazol-3-yl)pyrimidine-2,4-diamine (**15c**, 0.23 g), morpholine (0.06 mL), and DIPEA (0.2 mL) in *n*-BuOH (5 mL) was heated at 110 °C for 48 h. The solvent was removed under reduced pressure and the residue purified by reverse-phase chromatography (5–35% MeCN/H₂O with 0.1% TFA, 15 min) to give the trifluoroacetate salt of the title compound (yield: 20%). ¹H NMR: (MeOD) 8.75 (br s, 2H), 6.09 (br s, 1H), 5.35–5.09 (m, 1H), 3.90–3.50 (m, 8H), 2.38 (br s, 3H), 1.66 (d, 3H). *m/z*: 434.

N²-[(1*S*)-1-(5-fluoropyrimidin-2-yl)ethyl]-N⁴-(5-methoxy-1*H*-pyrazol-3-yl)-6-morpholin-4-ylpyrimidine-2,4-diamine (16d). A mixture of 6-chloro-*N*²-[(1*S*)-1-(5-fluoropyrimidin-2-yl)ethyl]-*N*⁴-(5-methoxy-1*H*-pyrazol-3-yl)pyrimidine-2,4-diamine (**15d**, 0.3 g), morpholine (0.09 mL), and DIPEA (0.2 mL) in *n*-BuOH (4 mL) was heated at 120 °C overnight. The solvent was removed under reduced pressure and the residue purified by reverse-phase chromatography (10–50% MeCN/H₂O with 0.1% TFA, 15 min) to give the trifluoroacetate salt of the title compound (yield: 50%). ¹H NMR: 11.97 (s, 1H), 9.49 (s, 1H), 8.80 (s, 2H), 7.58 (s, 1H), 5.20–4.98 (m, 3H), 3.72 (s, 3H), 3.53 (br s, 4H), 3.18 (br s, 4H), 1.49 (d, 3H). *m/z*: 416.

5-fluoro-N²-[(1*S*)-1-(5-fluoropyrimidin-2-yl)ethyl]-N⁴-(5-methoxy-1*H*-pyrazol-3-yl)-6-morpholin-4-ylpyrimidine-2,4-diamine (16e). A mixture of (*S*)-1-(5-fluoropyrimidin-2-yl)ethanamine hydrochloride (**8**) (0.2 g), 2-chloro-5-fluoro-*N*-(5-methoxy-1*H*-pyrazol-3-yl)-6-morpholin-4-ylpyrimidin-4-amine (**17b**, 0.4 g), and DIPEA (0.5 mL) in *n*-BuOH (2.5 mL) was heated in a sealed vessel at 170 °C for 24 h. The solvent was removed under reduced pressure, and the residue was purified by reverse-phase chromatography (2–40% MeCN/H₂O with 0.1% TFA, 15 min) to give the trifluoroacetate salt of the title compound (yield: 13%). ¹H NMR: 10.07 (s, 1H), 8.86 (s, 2H), 5.48 (s, 1H), 5.00 (m, 1H), 3.86 (s, 3H), 3.62–3.38 (m, 8H), 1.48 (d, 3H). *m/z*: 434.

5-chloro-N²-[(1*S*)-1-(5-fluoropyrimidin-2-yl)ethyl]-N⁴-(5-methoxy-1*H*-pyrazol-3-yl)-6-morpholin-4-ylpyrimidine-2,4-diamine (16f). A mixture of 5,6-dichloro-*N*²-[(1*S*)-1-(5-fluoropyrimidin-2-yl)ethyl]-*N*⁴-(5-methoxy-1*H*-pyrazol-3-yl)pyrimidine-2,4-diamine (**15f**, 0.1 g), morpholine (0.03 mL), and DIPEA (0.07 mL) in *n*-BuOH (2 mL) was heated in a sealed vessel at 150 °C for 24 h. The solvent was removed under reduced pressure, and the residue was purified by reverse-phase chromatography (2–40% MeCN/H₂O with 0.1% TFA, 15 min) to give the trifluoroacetate salt of the title compound (yield: 20%). ¹H NMR: 11.99 (s, 1H), 9.30 (s, 1H), 8.82 (s, 2H), 7.89 (d, 1H), 5.49 (s, 1H), 5.14–4.93 (m, 1H), 3.75 (s, 3H), 3.44–3.62 (m, 4H), 3.09–3.27 (m, 4H), 1.47 (d, 3H). *m/z*: 450.

Methyl Dimethylthiocarbamate (18). Dimethylamine (2 M in THF, 60 mL) was cooled at 0 °C and carbon disulfide (6 mL) added portionwise, followed by an aqueous solution of NaOH (4.8 g)/H₂O (40 mL). The reaction mixture was stirred at 0 °C for 30 min and subsequently at room temperature for 2 h. The reaction mixture was then recooled at 0 °C, and methyl iodide (7.5 mL) was added slowly. The resulting reaction mixture was stirred at 0 °C for 1 h, and then at room temperature overnight. The mixture was diluted with diethyl ether (100 mL) and extracted from the aqueous layer. The organic extracts were combined and dried over MgSO₄. Removal of the volatiles

under reduced pressure afforded the title compound (yield: quantitative) as white solid. ¹H NMR (CDCl₃): 3.52 (s, 3H), 3.35 (s, 3H), 2.61 (s, 3H).

(2*E* and 2*Z*)-3-(Dimethylamino)-3-(methylthio)acrylonitrile (19). Acetonitrile (12 mL) in THF (100 mL) was cooled at –78 °C and *n*-BuLi (2.5 M in hexane, 92 mL) was added dropwise through an addition funnel. The reaction was allowed to stir for 30 min at –78 °C, and then methyl dimethylthiocarbamate (**18**, 14.1 g) was added in one portion. The resulting mixture was stirred at –78 °C for 30 min and subsequently at room temperature for 6 h. The reaction mixture was then cooled at 0 °C, and methyl iodide (10 mL) was added. The reaction mixture was allowed to warm to room temperature and stirred at room temperature overnight. The mixture was diluted with ethyl acetate (200 mL), and the organic layer was washed with water (2 × 100 mL). The organic phase was concentrated under reduced pressure to give a residue which was purified by flash column chromatography with gradient 0–20% ethyl acetate in hexanes to afford the title compound (yield: 74%) as a mixture of *E* and *Z* isomers. ¹H NMR (major isomer) (CDCl₃): 4.08 (s, 1H), 3.00 (s, 6H), 2.39 (s, 3H).

5-chloro-N²-[(1*R*)-1-(5-fluoropyrimidin-2-yl)ethyl]-N⁴-(5-methyl-1*H*-pyrazol-3-yl)pyrimidine-2,4-diamine (21). A mixture of 1-(5-fluoropyrimidin-2-yl)ethanamine hydrochloride *rac*-**(8)** (0.1 g), 2,5-dichloro-*N*-(5-methyl-1*H*-pyrazol-3-yl)pyrimidin-4-amine (**7e**, 0.2 g), and DIPEA (0.15 mL) in *n*-BuOH (2.5 mL) was heated in a sealed microwave vessel in a microwave reactor at 180 °C for 6 h. The solvent was removed under reduced pressure and purified by reverse-phase chromatography (10–50% MeCN/H₂O with 0.1% TFA, 15 min) to give the trifluoroacetate salt of 5-chloro-*N*²-[1-(5-fluoropyrimidin-2-yl)ethyl]-*N*⁴-(5-methyl-1*H*-pyrazol-3-yl)pyrimidine-2,4-diamine **20** (yield: 19%).

The racemic mixture was resolved using chiral SFC. Column and solvent conditions: Column: Chiralpak AD-H, 250 × 20 mm. Modifier: 30% isopropanol, 0.1% dimethylethylamine. Flow rate: 60 mL/min. Oven: 40 °C. Outlet: 100 bar. Post-purification purity check: Chiral SFC using ultraviolet diode array. Column: Chiralcel AD-H, 250 × 4.6 mm. Conditions: 20% isopropanol, 0.1% dimethylethylamine. Flow rate: 3 mL/min; 15 min. Oven: 35 °C. Outlet: 120 bar.

9e was eluted first with a retention time of 11.3 min, as detected by an ultraviolet diode array detector. **21** eluted second with a retention time of 13.9 min, as detected by an ultraviolet diode array detector. Enantiomeric excess for **9e** (retention time 2.5 min) was >98% and for **21** (retention time 14.0 min) was estimated to be ~97%, using peak area percentage at 254 nm.

Analytical data for **21**: ¹H NMR (300 MHz): 12.03 (s, 1H), 8.83 (s, 2H), 7.88 (s, 1H), 7.44 (s, 1H), 5.93 (s, 1H), 4.92–5.29 (m, 1H), 2.20 (s, 3H), 1.49 (d, 3H). *m/z*: 350.

Rat Microsome Stability Assay. This primary in vitro test was carried out to assess the propensity of a compound to be metabolized by rat liver microsomal enzymes. The time-dependent disappearance of compound (2 μM initial concentration) incubated with microsomes was measured using LCMS/MS. Results are reported as intrinsic clearance of compound (CL_{int}, in μL/min/mg protein).

Log D Measurement. The octanol–water partition coefficient (log *D*) is measured using the shake flask method. Aliquots of test compound stock solution were added to a mixture of phosphate buffer at pH 7.4 and *n*-octanol. The test compounds were allowed to distribute between the two phases by shaking samples at 1200 rpm, at 25 °C, for 1 h. Concentration of test compounds in each of the two phases was analyzed using an HPLC-UV with MS confirmation.

Aqueous Equilibrium Solubility Assay. This primary in vitro test assesses the equilibrium solubility of a compound in pH 7.4 phosphate buffer. Solid compound was prepared by evaporation of a DMSO solution. Dried compound was incubated for 24 h with agitation in buffer at 25 °C. Undissolved compound was removed by filtration, and the concentration of test

compound in the filtrate was measured by HPLC-UV, with MS confirmation, and calculated against a one-point standard. The lower and higher limits of quantification for this assay were 1 and 1000 μM , respectively.

Aurora A Assay. This in vitro test was used for measuring the change of DNA content in flow cytometry during the compound treatment. Cells were plated on day 1 at established seeding density. **9e** and controls were added on day 2 at required time points, and cells were harvested and fixed in ice-cold 70% ethanol. The fixed cells were resuspended in permeabilization buffer (PBS with 0.05% Triton X-100) for 10 min and washed with wash buffer (PBS with 1% BSA) once. Cells were then incubated with 1:500 dilution of antiphosphorylated histone H3 for 2 h in the dark and followed by the incubation of 1:500 dilution of Alexa Fluor 488 goat antirabbit IgG for 2 h in the dark. Cells were washed once after the incubation of each antibody. Cells were then incubated with PI staining solution (PBS with 40 $\mu\text{g}/\text{mL}$ PI and 100 $\mu\text{g}/\text{mL}$ RNase I) at 37 °C for 30 min. Cells were analyzed on a flow cytometer.

Mouse Allograft Tumor Models, Pharmacodynamic Studies, and Bioluminescence Imaging. Female, NC_r nude mice (Taconic Farms, Germantown, NY, USA) were purchased at 5–6 weeks of age and maintained under specific-pathogen-free conditions in an AAALAC-accredited facility. Animal protocols were approved by the AstraZeneca R&D Boston Institutional Animal Care and Use Committee. All animal work was conducted in accordance with applicable internal standards and external local and national guidelines, regulations, and legislation. Animals were acclimated in-house for a period of 3 days prior to cell implantation.

Mouse BaF3 cells expressing TEL-Jak2 fusion protein were maintained in RPMI 1640 medium supplemented with 10% fetal bovine serum (HyClone) and L-glutamine (Gibco). One million cells in 0.1 mL of sterile PBS were injected into the mouse lateral tail vein. Single-dose pharmacodynamic studies were carried out 10 days post-tumor cell implantation. **9e** was dissolved in 0.5% HPMC and 0.1% Tween80 (pH ~2) and dosed by oral gavage to the tumor bearing mice. Mice were sacrificed at 2, 4, 6, 8, and 12 h after drug administration. Spleen samples were collected to assess phospho-Stat5 levels by Western blot as described previously.¹⁴

For tumor growth inhibition studies, one million BaF/3 TEL-Jak2-luc cells in 0.1 mL of sterile PBS were injected into the mouse lateral tail vein. To track tumor burden in mice, in vivo bioluminescent imaging was performed using the IVIS 200 instrument (Caliper LifeSciences) on days 1, 4, 7, and 9 post-tumor cell implantation. Before imaging, mice received an intraperitoneal dose of d-luciferin (150 mg/kg in PBS; Caliper LifeSciences), and were anesthetized with 2.5–3% isoflurane. Images were acquired with *LivingImage* software (v 2.5, Caliper LifeSciences) 10 min after d-luciferin injection. The imaging data from day 1 was used to randomize the animals into experimental groups. Dosing commenced on day 3 with animals receiving vehicle or **9e**. Mice were dosed by oral gavage twice daily for a total of 7 days.

Protein Expression, Purification, Crystallization, and Structure Determination. Human Jak2 was modeled in Quanta 2000²⁴ using a JAK3 protein structure¹⁸ (pdb entry: 1YVJ). Using this model (not detailed), construct termini and areas for potential surface entropy reduction were identified. Human 6-His-Jak2 (residues 835–1132) with mutations K943A and K945A was cloned into pT7 3.3 vector using Gateway cloning (Invitrogen). Protein was expressed in BL21* cells grown in Terrific Broth media in the presence of tetracycline (12.5 $\mu\text{g}/\text{mL}$). Expression was induced at OD₆₀₀ 0.6 with 0.1 mM isopropyl β -D-1-thiogalactopyranoside (IPTG). Following induction with IPTG, cells were incubated at 18 °C for 20 h before harvesting. Cells were resuspended in Buffer A (20 mM Tris pH 7.9, 250 mM NaCl, 10 mM imidazole, 1 mM tris(2-carboxyethyl)phosphine) supplemented with EDTA-free Complete Protease inhibitors (Roche) and 2 μM staurosporine (Sigma). Cells were lysed using a cell

disruptor (Constant Systems Basic Z). The supernatant was loaded onto a NiNTA affinity column (Qiagen). After washing with Buffer A, the protein was eluted with Buffer A plus 300 mM imidazole. Fractions containing 6His-Jak2 were pooled and 5 mM DTT, Lambda phosphatase (Upstate), and TEV protease were added to the protein and left to incubate overnight at 4 °C. The cleaved protein was exchanged into a low salt buffer (20 mM Tris pH 8.5, 25 mM NaCl, 1 mM dithiothreitol (DTT)) using an XK26 fast desalting column (GE Healthcare) before loading onto a Resource Q ion-exchange column (GE Healthcare) equilibrated in low salt buffer. Bound protein was eluted by increasing the NaCl concentration to 1 M. Fractions containing Jak2 were pooled and incubated with 60 μM staurosporine on ice for 15 min before buffer exchanging into 20 mM Tris pH 8.5, 100 mM NaCl, 1 mM DTT using a Superdex S-75 size exclusion chromatography column (GE Healthcare). The Jak2–staurosporine complex was concentrated to 8.7 mg/mL for crystallization.

Crystals of Jak2–staurosporine complex were grown using the hanging drop method at 293 K. The reservoir solution contained 28% w/v Peg3350, 200 mM ammonium acetate, 100 mM sodium citrate, pH 6.0. Drops were set up with 1.5 μL protein and 1 μL reservoir. Trays were incubated at 20 °C and bipyramidal crystals appeared after 3–6 days. Jak2–staurosporine crystals were soaked in well solution with 5 mM of compound **9e** and 5% DMSO for 30 h at 20 °C. Crystals were then cryoprotected using well solution containing an additional 10% glycerol. Crystals were frozen directly into a cryostream at 100 K. Diffraction data were collected at ESRF beamline ID23-EH2 equipped with an ADSC Quantum 4 CCD X-ray detector, using a Si111 monochromated wavelength of 0.873 Å. Data were processed using MOSFLM and SCALA and reduced using CCP4 software.²⁵ The structures were solved by molecular replacement using coordinates of the Jak2 kinase domain²⁶ as a trial model using CCP4 software. Protein and inhibitor were modeled into the electron density using COOT²⁷ and AFITT.²⁸ The model was refined using Refmac.²⁹ Atomic coordinates and structure factors for the human Jak2 complex with compound **9e** have been deposited in the Protein Data Bank (2XA4) together with structure factors and detailed experimental conditions.

Crystallographic statistics for the Jak2/compound **9e** complex are as follows, with statistics for the highest-resolution shell in brackets: Space group C2, unit cell 43.9, 126.7, 134.3 Å, β 97.0, Resolution 33.33–2.04 (2.09–2.04) Å, 43209 (3016) unique reflections with an overall redundancy of 3.0 (2.9) give 93.4 (87.2%) completeness with R_{merge} of 7.0 (40.4%) and mean $I/\sigma(I)$ of 10.3 (1.6). The final model containing 4451 protein, 308 solvent, and 48 compound atoms has an R -factor of 19.72% (R_{free} 24.46%) using 5% of the data. Mean temperature factors for the protein and the ligand are 32 and 33 Å², respectively. Pictures of the crystal structure of **9e** with Jak2 kinase have been generated by Pymol.³⁰

Acknowledgment. The authors would like to thank Nancy DeGrace and Kanayochukwu Azogu for chiral separations, David Scott for analysis of early screening data, David Ayres for PK sample analysis, Clare Williams for helping with reagent supply for protein isolation, Richard Mott for initial protein work, and Mark McAlister for initiating structural work. Special thanks to Susan Ashwell and John Habermann for useful discussions during the preparation of this manuscript.

Supporting Information Available: Figures S1–S4. This material is available free of charge via the Internet at <http://pubs.acs.org>.

References

- (1) Yamaoka, K.; Saharinen, P.; Pesu, M.; Holt, V. E. T., III; Silvennoinen, O.; O'Shea, J. J. The Janus kinases (Jaks). *Genome Biol.* **2004**, 5, 253.

- (2) Levine, R. L.; Wadleigh, M.; Cools, J.; Ebert, B. L.; Wernig, G.; Huntly, B. J. P.; Boggon, T. J.; Wlodarska, I.; Clark, J. J.; Moore, S.; Adelsperger, J.; Koo, S.; Lee, J. C.; Gabriel, S.; Mercher, T.; D'Andrea, A.; Fröhling, S.; Döhner, K.; Marynen, P.; Vandenberghe, P.; Mesa, R. A.; Tefferi, A.; Griffin, J. D.; Eck, M. J.; Sellers, W. R.; Meyerson, M.; Golub, T. R.; Lee, S. J.; Gilliland, D. G. Activating mutation in the tyrosine kinase JAK2 in polycythemia vera, essential thrombocythemia, and myeloid metaplasia with myelofibrosis. *Cancer Cell* **2005**, *7*, 387–397.
- (3) James, C.; Ugo, V.; Le Couédic, J. P.; Staerk, J.; Delhommeau, F.; Lacout, C.; Garçon, L.; Raslova, H.; Berger, R.; Bennacaour-Griselli, A.; Villeval, J. L.; Constantinescu, S. N.; Casadevall, N.; Vainchenker, W. A unique clonal JAK2 mutation leading to constitutive signaling causes polycythemia vera. *Nature* **2005**, *434*, 1144–1148.
- (4) Baxter, E. J.; Scott, L. M.; Campbell, P. J.; East, C.; Fourouclas, N.; Swanton, S.; Vassiliou, G. S.; Bench, A. J.; Boyd, E. M.; Curtin, N.; Scott, M. A.; Erber, W. N.; the Cancer Genome project; Green, A. R. Acquired mutation of the tyrosine kinase JAK2 in human myeloproliferative disorders. *Lancet* **2005**, *365*, 1054–1061.
- (5) Levine, R. L. Mechanisms of mutations in myeloproliferative neoplasms. *Best Pract. Res. Clin. Haematol.* **2009**, *22*, 489–494.
- (6) Quintás-Cardama, A.; Vaddi, K.; Liu, P.; Manshouri, T.; Li, J.; Scherle, P. A.; Caulder, E.; Wen, X.; Li, Y.; Wetzl, P.; Rupar, M.; Burn, T.; Lo, Y.; Kelley, J.; Covington, M.; Shepard, S.; Rodgers, J. D.; Haley, P.; Kantarjian, H.; Fridman, J. S.; Verstovsek, S. Preclinical characterization of the selective JAK1/2 inhibitor INCB018424: therapeutic implications for the treatment of myeloproliferative neoplasms. *Blood* **2010**, *115*, 3109–3117.
- (7) Wernig, G.; Kharas, M. G.; Okabe, R.; Moore, S. A.; Leeman, D. S.; Cullen, D. E.; Gozo, M.; McDowell, E. P.; Levine, R. L.; Doukas, J.; Mak, C. C.; Noronha, G.; Martin, M.; Ko, Y. D.; Lee, B. H.; Soll, R. M.; Tefferi, A.; Hood, J. D.; Gilliland, D. G. Efficacy of TG101348, a selective JAK2 inhibitor, in treatment of a murine model of JAK2V617F-induced polycythemia vera. *Cancer Cell* **2008**, *13*, 311–320.
- (8) Burns, C. J.; Bourke, D. G.; Andrau, L.; Bu, X.; Charman, S. A.; Donohue, A. C.; Fantino, E.; Farrugia, M.; Feutrell, J. T.; Joffe, M.; Kling, M. R.; Kurek, M.; Nero, T. L.; Nguyen, T.; Palmer, J. T.; Phillips, I.; Shackleford, D. M.; Sikanyik, H.; Styles, M.; Su, S.; Treutlein, H.; Zeng, J.; Wilks, A. F. Phenylaminopyrimidines as inhibitors of Janus kinases (JAKs). *Bioorg. Med. Chem. Lett.* **2009**, *19*, 5887–5882.
- (9) Hexner, E. O.; Serdikoff, C.; Jan, M.; Swider, C. R.; Robinson, C.; Yang, S.; Angeles, T.; Emerson, S. G.; Carroll, M.; Ruggeri, B.; Dobrzanski, P. Lestaurtinib (CEP701) is a JAK2 inhibitor that suppresses JAK2/STAT5 signaling and the proliferation of primary erythroid cells from patients with myeloproliferative disorders. *Blood* **2008**, *111*, 5663–5671.
- (10) Plo, I.; Vainchenker, W. Molecular and genetic bases of myeloproliferative disorders: questions and perspectives. *Clin. Lymphoma, Myeloma Leukemia* **2009**, *9* (Suppl.3), S329–S339.
- (11) Wang, T.; Lamb, M. L.; Scott, D. A.; Wang, H.; Block, M. H.; Lyne, P. D.; Lee, J. W.; Davies, A. M.; Zhang, H.; Zhu, Y.; Gu, F.; Han, Y.; Wang, B.; Mohr, P. J.; Kaus, R. J.; Josey, J. A.; Hoffmann, E.; Thress, K.; MacIntyre, T.; Wang, H.; Omer, C. A.; Yu, D. Identification of 4-aminopyrazolopyrimidines as potent inhibitors of Trk kinases. *J. Med. Chem.* **2008**, *51*, 4672–4684.
- (12) Baasner, B.; Klauke, E. A new route to the synthesis of 5-fluorouracil. *J. Fluorine Chem.* **1989**, *45*, 417–430.
- (13) Gozgit, J. M.; Bebernitz, G.; Patil, P.; Ye, M.; Wu, J.; Su, N.; Wang, T.; Ioannidis, S.; Davies, A. M.; Huszar, D.; Zinda, M. Effects of the JAK2 inhibitor, AZ960, on Pim/BAD/BCL-xL survival signaling in the human JAK2 V617F cell line SET-2. *J. Biol. Chem.* **2008**, *283*, 32334–32343.
- (14) Ioannidis, S.; Lamb, M. L.; Davies, A. M.; Almeida, L.; Su, M.; Bebernitz, G.; Ye, M.; Bell, K.; Alimzhanov, M.; Zinda, M. Discovery of pyrazol-3-ylamino pyrazines as novel JAK2 inhibitors. *Bioorg. Med. Chem. Lett.* **2009**, *19*, 6524–6528. See also for the use of high versus low ATP concentration Knight, A. Z.; Shokat, K. M. Features of selective kinase inhibitors. *Chem. Biol.* **2005**, *12*, 621–637.
- (15) Compound **9g** displayed good activity in an EPOR Stat5 cellular assay, EC₅₀ = 0.039 mM. For more details about the assay see ref 16.
- (16) Ioannidis, S.; Lamb, M. L.; Almeida, L.; Guan, H.; Peng, B.; Bebernitz, G.; Bell, K.; Alimzhanov, M.; Zinda, M. Replacement of pyrazol-3-yl amine hinge binder with thiazol-2-yl amine: Discovery of potent and selective JAK2 inhibitors. *Bioorg. Med. Chem. Lett.* **2010**, *20*, 1669–1673.
- (17) Guan, H.; Hayter, B. R.; Huang, S.; Ioannidis, S.; Johannes, J.; Lamb, M.; Peng, B.; Yang, B. Preparation of pyrazolyl-amino-substituted pyrimidines and their use for the treatment of cancer. WO2008132502, 2008.
- (18) Boggon, T. J.; Li, Y.; Manley, P. W.; Eck, M. J. Crystal structure of the Jak3 kinase domain in complex with a staurosporine analog. *Blood* **2005**, *106*, 996–1002.
- (19) Hedvat, M.; Huszar, D.; Herrmann, A.; Gozgit, J. M.; Schroeder, A.; Sheehy, A.; Buettner, R.; Proia, D.; Kowollik, C. M.; Xin, H.; Armstrong, B.; Bebernitz, G.; Weng, S.; Wang, L.; Ye, M.; McEachern, K.; Chen, H.; Morosini, D.; Bell, K.; Alimzhanov, M.; Ioannidis, S.; McCook, P.; Cao, Z. A.; Yu, H.; Jove, R.; Zinda, M. The JAK2 inhibitor AZD1480 potently blocks Stat3 signaling and oncogenesis in solid tumors. *Cancer Cell* **2009**, *16*, 487–497.
- (20) Mortlock, A. A.; Foote, K. M.; Heron, N. M.; Jung, F. H.; Pasquet, G.; Lohmann, J.-J. M.; Warin, N.; Renaud, F.; De Savi, C.; Roberts, N. J.; Johnson, T.; Dousson, C. B.; Hill, G. B.; Perkins, D.; Hatter, G.; Wilkinson, R. W.; Wedge, S. R.; Heaton, S. P.; Odedra, R.; Keen, N. J.; Crafter, C.; Brown, E.; Thompson, K.; Brightwell, S.; Khatri, L.; Brady, M. C.; Kearney, S.; McKillop, D.; Rhead, S.; Parry, T.; Green, S. Discovery, synthesis, and in vivo activity of a new class of pyrazolylamino quinazolines as selective inhibitors of Aurora B Kinase. *J. Med. Chem.* **2007**, *50*, 2213–2224.
- (21) Thress, K.; MacIntyre, T.; Wang, H.; Whitston, D.; Liu, Z.-Y.; Hoffmann, E.; Wang, T.; Brown, J. L.; Webster, K.; Omer, C.; Zage, P. E.; Zeng, L.; Zweidler-McKay, P. A. Identification and preclinical characterization of AZ-23, a novel, selective, and orally bioavailable inhibitor of the Trk kinase pathway. *Mol. Cancer Ther.* **2009**, *8*, 1818–1827.
- (22) Quentmeier, H.; MacLeod, R. A.; Zaborski, M.; Drexler, H. G. JAK2V617 tyrosine kinase mutation in cell lines derived from myeloproliferative disorders. *Leukemia* **2006**, *20*, 471–476.
- (23) Rehemtulla, A.; Stegman, L. D.; Cardozo, S. J.; Gupta, S.; Hall, D. E.; Contag, C. H.; Brian D Ross, B. D. Rapid and quantitative assessment of cancer treatment response using *in vivo* bioluminescence imaging. *Neoplasia* **2000**, *2*, 491–495.
- (24) QUANTA, Release 2000, San Diego: Accelrys Inc., 2000.
- (25) Collaborative Computational Project Number 4. The CCP4 suite: programs for protein crystallography. *Acta Crystallogr.* **1994**, *D50*, 760–763.
- (26) Lucet, I. S.; Fantino, E.; Styles, M.; Bamert, R.; Patel, O.; Broughton, S. E.; Walter, M.; Burns, C. J.; Treutlein, H.; Wilks, A. F.; Rossjohn, J. The structural basis of Janus kinase 2 inhibition by a potent and specific pan-Janus kinase inhibitor. *Blood* **2006**, *107*, 176–183.
- (27) COOT: Emsley, P.; Lohkamp, B.; Scott, W.; Cowtan, K. *Acta Crystallogr.* **2010**, *D66*, 486–501.
- (28) AFITT: OpenEye Scientific Software, Inc., Santa Fe, NM, USA, www.eyesopen.com.
- (29) Refmac v 5.1.17: Murshudov, G. N.; Vagin, A. A.; Dodson, E. J. *Acta Crystallogr.* **1997**, *D53*, 240–255.
- (30) DeLano, W. L. The PyMOL molecular graphics system; DeLano Scientific: San Carlos, CA, USA, 2002; http://www.pymol.org.